Ore Geology Reviews 86 (2017) 79–99

Contents lists available at ScienceDirect

Ore Geology Reviews

journal homepage: www.elsevier.com/locate/oregeo

Mineral chemistry and genesis of the Permian Cihai and Cinan magnetite deposits, Beishan, NW China

Dongmei Tang [a,*], Kezhang Qin [a,*], Bo Chen [a], Yajing Mao [a], Hu Guo [b], Noreen J. Evans [c]

[a] Key Laboratory of Mineral Resources, Institute of Geology and Geophysics, Chinese Academy of Sciences, Beijing 100029, China
[b] Tianjin Geological Research Center, Geological Survey of China, Tianjin 300170, China
[c] John de Laeter Center, TIGeR, Applied Geology, Curtin University, Perth, WA 6845, Australia

ARTICLE INFO

Article history:
Received 21 August 2016
Accepted 19 January 2017
Available online 21 January 2017

Keywords:
Cihai and Cinan mafic intrusions
Clinopyroxene
Magnetite
Mineralization mechanism
Central Asian Orogenic Belt

ABSTRACT

Cihai and Cinan are Permian magnetite deposits related to mafic-ultramafic intrusions in the Beishan region, Xinjiang, NW China. The Cihai mafic intrusion is dominantly composed of dolerite, gabbro and fine-grained massive magnetite ore, while gabbro, pyrrhotite + pyrite-bearing clinopyroxenite and magnetite ore comprise the major units in Cinan. Clinopyroxene occurs in both deposits as 0.1–2 mm in diameter subhedral to anhedral grains in dolerite, gabbro and clinopyroxenite. High FeO contents (11.7–28.9 wt%), low SiO_2 (43.6–54.3 wt%) and Al_2O_3 contents (0.15–6.08 wt%), and low total REE and trace element contents of clinopyroxene in the Cinan clinopyroxenite imply crystallization early, at high pressure. This clinopyroxene is FeO-rich and Si and Ti-poor, consistent with the clinopyroxene component of large-scale Cu-Ni sulfide deposits in the Eastern Tianshan and Panxi ares, as well as Tarim mafic intrusion and basalt, implying the Cinan mafic intrusion and sulfide is related to tectonic activity in the Tarim LIP. The similar mineral chemistry of clinopyroxene, apatite and magnetite in the Cihai and Cinan gabbros (e.g., depleted LREE, negative Zr, Hf, Nb and Ta anomalies in clinopyroxene, lack of Eu anomaly in apatite and similarity of oxygen fugacity as indicated by V in magnetite), indicate similar parental magmatic characteristics. Mineral compositions suggest a crystallization sequence of clinopyroxenite/with a small amount of sulfide – gabbro – magnetite ore in the Cinan deposit, and magnetite ore – gabbro – dolerite in Cihai. The basaltic magma was emplaced at depth, with magnetite segregation (and formation of the Cinan magnetite ores) occurring in relatively low fO_2 conditions, after clinopyroxenite and gabbro fractional crystallization. The evolved Fe-rich basaltic magma rapidly rose to intermediate or shallow depths, forming an immiscible Fe-Ti oxide magma as fO_2 increased and leaving a Fe-poor residual magma in the chamber. The residual magmas was emplaced at different levels in the crust, forming the Cihai gabbro and dolerite, respectively. Finally, the immiscible Fe-Ti oxide magma was emplaced into the earlier formed dolerite because of late magma pulse uplift, resulting in a distinct boundary between the magnetite ores and dolerite.

1. Introduction

Magmatic Fe-Ti oxide deposits are mainly associated with two types of rock: (i) large layered mafic-ultramafic intrusions where ore-bearing rocks are either gabbro without ultramafic rocks, such as at the Panzhihua, Baima and Taihe deposits in southwest China (Zhou et al., 2005; Pang et al., 2008; Shellnutt et al., 2009) or a combination of mafic and ultramafic rocks, such as at the Bushveld layered complex in South Africa (Naldrett, 1999), Duluth intrusion in the USA (Ripley, 1981), Jameson Range in the central Australia (Karykowski et al., 2016), Xinjie and Hongge deposits in southwest China (Zhong et al., 2002, 2006); and (ii) anorthosites, where the rock assemblage is generally plagioclase-gabbro-norite-monzonite-charnockite (AMCG) (Kerr and Ryan, 2000), such as in the Tellnes Fe oxide deposit in Norway (Wilmart et al., 1989), Lac Tio Fe-Ti deposits in Canada (Ashwal, 1993), Damiao V-Ti-Fe oxide deposit in China, Windimurra deposit in Australia, and Rooiwater and Ushwana deposit in South Africa (Reynolds, 1980; Lee, 1996).

Many mechanisms have been proposed to explain the petrogenesis of mafic-related iron ore deposits including gravity segregation (Emmons, 1904; Charlier et al., 2006), fractional segregation (Obsorne, 1959; Cawthorn and McCarthy, 1980), magma mixing, assimilation or contamination (Harney et al., 1990), magma immiscibility (Duchesne, 1999; Charlier and Grove, 2012; Lester et al.,

* Corresponding authors.
E-mail addresses: tangdm1981@126.com (D. Tang), kzq@mail.iggcas.ac.cn (K. Qin).

http://dx.doi.org/10.1016/j.oregeorev.2017.01.019
0169-1368/

2013; Liu et al., 2014; Wang et al., 2008), and change of oxygen fugacity conditions (Klemm et al., 1985; Karkkainen and Appelqvist, 1999). In fact, large deposits might have been generated by some combination of these factors.

The Beishan area, at the southern margin of the Central Asian Orogenic Belt (CAOB), is located in the northeastern part of the Tarim Block and adjacent to the Middle Tianshan Massif (Fig. 1a). During the prolonged orogenic events associated with the collision between the Junggar and Tarim blocks in the Paleozoic, a suite of mafic-ultramafic rocks (267–285 Ma; Su et al., 2011; Xue et al., 2016) that typically host magmatic Cu-Ni and Pt ore deposits, were emplaced along the ENE axis in the Beishan area (Jiang et al., 2006; Su et al., 2011, 2015; Xia et al., 2013; Xue et al., 2016) (Fig. 1b). In recent years, several Fe deposits have also been discovered including the Cihai and Cinan deposits, both located in the Cihai mining district, Beishan. Zircon U-Pb dating of Fe deposits has yielded ages of 264–295 Ma (Xue et al., 2000; Qi et al., 2012; Huang et al., 2013; Meng et al., 2014; Chen et al., 2015) and, in fact, many studies have documented mineralization coeval with dolerite and gabbro (the major intrusions) in the Cihai and Cinan deposits (Tang et al., 2012; Hou et al., 2013; Meng et al., 2014). In the northwest area of the Tarim Block, there are many Permian (269–282 Ma, Cao et al., 2014) Fe oxide deposits associated with mafic intrusions, including the Wajlitage and Piqiang V-Ti magnetite deposits. However, the genetic relationship between these Permian deposits and intrusions in Tarim basin and the coeval Cihai and Cinan Fe deposits and related mafic intrusion has not yet clear.

The mineralization mechanisms that have been proposed for the Cihai deposit include magmatic, magmatic and hydrothermal metasomatism, and skarn genesis (Tang et al., 2010; Qi et al., 2012; Huang et al., 2013; Meng et al., 2014). The formation age of the Cihai and Cinan mafic–ultramafic rocks are similar, and they both contain Fe ores. However, as the Cinan deposit also contains Cu-Ni sulfide, it is unclear as to whether all of the oxide and sulfide originated from the same metallogenic system. The genetic relationships between the sulfide and oxide deposits, and between the deposits and mafic intrusions, remain essentially unknown.

Primary and accessory minerals (e.g., clinopyroxene, magnetite and apatite) can be used to understand the tectonic setting, mineralization mechanism(s), and physical and geochemical conditions of host rock formation (Nimis and Ulmer, 1998; Belousova et al., 2002; Downes et al., 2003; Yogodzinski and Kelemen, 2007; Driouch et al., 2010; Bonnetti et al., 2015). CaO contents of clinopyroxene have related to temperature, while several oxides have been used for pressure calculation (Brey and Kohler, 1990; Nimis and Ulmer, 1998), and SiO_2 and Al_2O_3 contents in clinopyroxene can indicate the magma characteristics (Kushiro, 1960). Magnetite may be a significant host for Fe, Mn, Al, Ti, V, Nb and Ta, and the concentrations of all lithophile elements (Cr, Ti, V, Al, Mn, Sc, Nb, Ga, Ge, Ta, Hf, W and Zr) are highest in the early-forming Fe oxide (Melluso et al., 2008; Dare et al., 2012). Magnetite is also an useful indicator of redox conditions (Knipping et al., 2015; Bonnetti et al., 2015).

In this study, we present new major oxide and trace element data from clinopyroxene, magnetite and apatite obtained from a variety of Cihai and Cinan samples in order to elucidate the structural setting and genesis of mafic-ultramafic rocks and ores and to unravel the mineralization processes and paragenetic relationships at the two deposits.

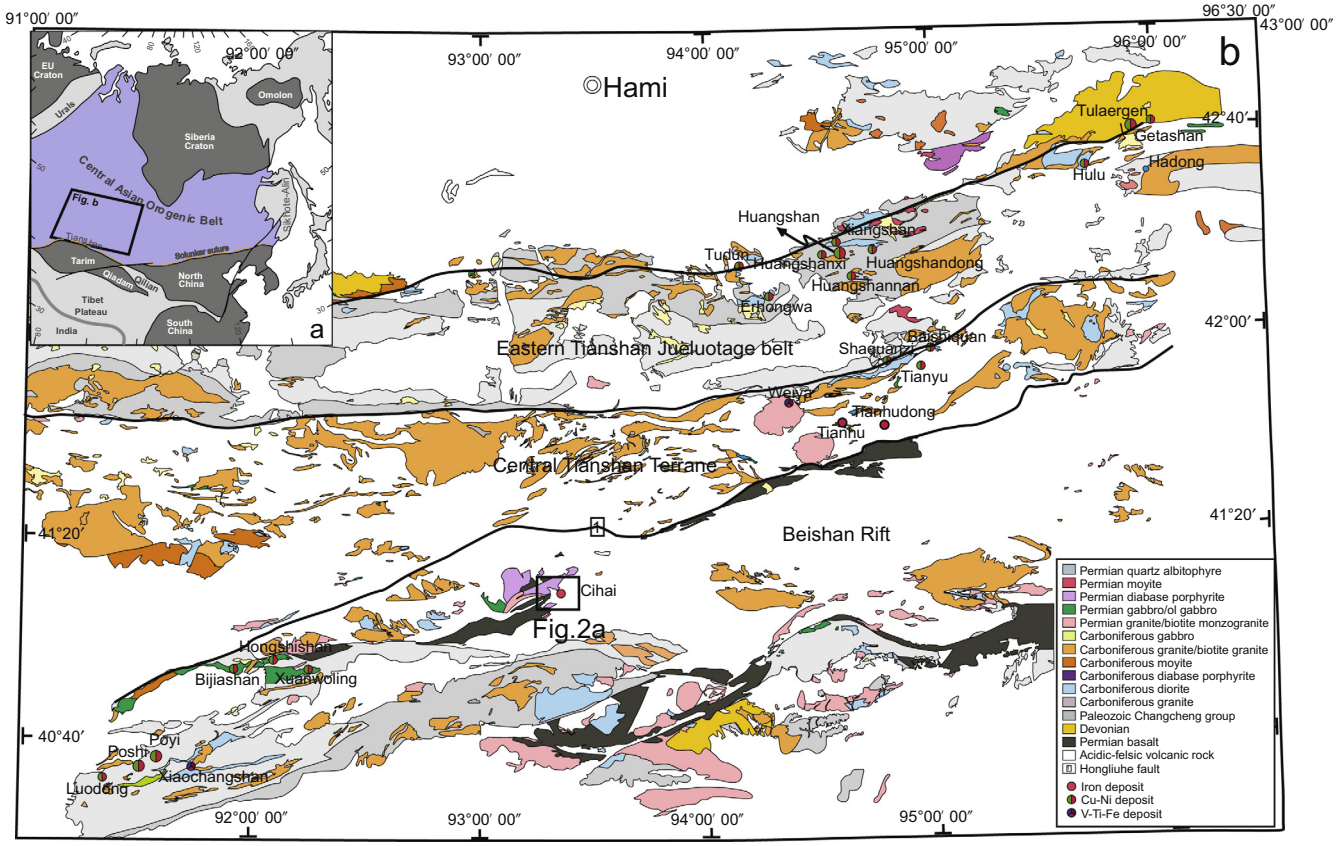

Fig. 1. (a) Tectonic units and location of Beishan region in Xinjiang, NW China, modified after Li et al. (2012). The tectonic units are based on Jahn et al. (2004) and Xiao et al. (2009). (b) Distribution of the Cihai mining camp in the Beishan region and coveal magatic Cu-Ni sulfide and Fe oxide deposits associated with mafic-ultramafic intrusions in the adjacent area, modified after Qin et al. (2003).

2. Geological background

The CAOB represents the world's largest Late Paleozoic orogenic belt and is located between the Siberian Craton in the north and the Tarim Craton and North China Craton in the south (Fig. 1a) (Xiao et al., 2004, 2013; Windley et al., 2007; Wong et al., 2010; Rojas-Agramonte et al., 2011). The Beishan area is at the conjunction of the CAOB and the Sino-Korean and Tarim cratons. It is located in the northeastern part of the Tarim Basin, adjacent to the Middle Tianshan Massif in the north (Fig. 1b; Xu et al., 2009) and is mainly composed of Precambrian crystalline basement and overlying sedimentary rocks, including the Beishan, Gutongjing, Yangjibulake, and Aierlanjigan groups. The Precambrian to Permian strata in the Beishan region are separated by well-developed fault-related uplifts and sags (Fig. 1b) (Su et al., 2011; Xu et al., 2009). Late Paleozoic tectonic evolution in this region was closely related to the subduction and subsequent closure of the South Tianshan Ocean (e.g., Gao et al., 1998, 2006, 2009; Xiao et al., 2003, 2004, 2009; Zhang et al., 2002). A rift developed in the Carboniferous and Permian, accompanied by intermediate-basic volcanic eruptions (Su et al., 2012). From west to east, the Permian mafic-ultramafic intrusion related magmatic Cu-Ni sulfide deposits that have been successively explored in the past two decades are: Luodong, Poshi, Poyi, Bijiashan, Hongshishan, and Xuanwoling (Fig. 1b). Permian mafic-related Fe-Ti oxide deposits are located in the Xiaochangshan and Cihai districts.

3. Geology of the Cihai and Cinan deposits

The Cihai ore district can be divided into three deposits: Cihai, Cinan and Cixi (Fig. 2a). All three are associated with Permian mafic-ultramafic intrusions and are located in the northern part of the Beishan area, bounded by the ENE trending secondary fault of the Hongliuhe Fault, near the northeast edge of the Tarim block (Li et al., 2008a). The ENE-trending faults, secondary faults and tight folds are the most well developed structures in the Beishan area. The stratum in the Cihai district mainly comprises Proterozoic Pingtoushan group and lower Permian rocks, which lay unconformably on the Pingtoushan group. Tertiary rocks occur sporadically, while Quaternary rocks are widely distributed in the Cihai ore district (Li et al., 2008a). Magmatic activity is mainly focused in the Variscan, with volcanic rocks including rhyolite, andesite and basalt, and intrusive dolerite, gabbro, olivine gabbro and clinopyroxenite (NGPBMMI, 1999). The Cihai deposit is operated as an open-pit mine (Fig. 2b), while the Cinan deposits are being mined underground. The Cixi deposit is strongly altered (and currently closed) so this study focuses on the Cihai and Cinan deposits where samples are fresher and more readily available.

3.1. Cinan intrusive rocks and orebody

The clinopyroxenite in the Cinan deposit contains 75–85 vol% clinopyroxene, with 10–15 vol% magnetite, and 1–5 vol% hornblende, calcite, ilvaite and apatite. The clinopyroxene grains are anhedral to subhedral and commonly range from 200 μm to 800 μm (larger than clinopyroxene at Cihai) (Fig. 3a, c and e). The gabbro contains 30–40 vol% clinopyroxene, 35–40 vol% plagioclase, 15–20 vol% magnetite and 5–10 vol% hornblende, plus minor apatite.

The Cinan clinopyroxenite and gabbro both contain magnetite mineralization and Cu-Ni sulfide (Fig. 3b, d, f and h), but magnetite mineralization is weaker than at Cihai, and Cu-Ni sulfide does not reach economic grades. While most of the magnetite ore is disseminated and net-textured (Fig. 4a and d), there are also enclaves of massive magnetite ore (Fig. 4b and c). Cu-Ni sulfides are mainly disseminated (Fig. 3b, d and f). The gabbro contains sparse disseminated pyrrhotite, pentlandite and chalcopyrite, and veinlet pyrite. Oxide and sulfide occur in some ore samples. The mineralized gabbro contains needles of ilmenite, while almost no ilmenite is found in clinopyroxenite (Fig. 4).

Dating of zircon from the Cinan gabbro yielded a SIMS age of 273.0 ± 1.9 Ma (Chen et al., 2015), while apatite from clinopyroxenite had a U-Pb age of 273.1 ± 2.3 Ma (Table 1, Chen et al., 2015). The formation ages of both the Cinan gabbro and clinopyroxenite are early Permian. Furthermore, the Cinan and Cihai intrusions are coeval with most sulfide-bearing mafic-ultramafic intrusions (and some basalt) in the Beishan region and adjacent area (Yang et al., 2006; Zhou et al., 2006; Pan et al., 2008; Zhang et al., 2010a,b; Su et al., 2011).

3.2. Cihai intrusive rocks and orebody

The Cihai complex consists of dolerite and gabbro with vein and ellipse-shaped magnetitite intruding the mafic rock nearly vertically. The iron orebody is contained within the dolerite and there are sharp and clear intrusive contacts between orebody and country rock (Fig. 2c and d). The surface exposure of the Cihai gabbro is diamond-shaped, ~7 km in length and 1.5–3 km in width, with a total outcrop area of 10.5–21 km^2 (Fig. 2a). The dolerite and gabbro were emplaced within Permian andesite, volcanic conglomerate and basalt, Neoproterozoic marble and quaternary sedimentary rocks. The intrusion has been dated by zircon U-Pb SIMS and pyrite re-Os methods, with the dolerite and gabbro unit yielding crystallization ages of 275 ± 2.2 Ma and 281.9 ± 3.2 Ma (Chen et al., 2015), respectively, while sulfide formation occurred at 262.3 ± 5.6 Ma (Huang et al., 2013).

The Cihai dolerite is altered, but the most weakly altered rocks contain euhedral, 200– 600 μm plagioclase crystals and interstitial, anhedral clinopyroxene grains (less than 200 μm) (Fig. 5a). The dolerite is composed of 50–65 vol% plagioclase, 15–25 vol% clinopyroxene, 1–5 vol% hornblende and apatite, with minor ilmenite and titanite (<vol 1%). The gabbro contains interlocking and randomly orientated tabular plagioclase and anhedral clinopyroxene (Fig. 5b), with minor hornblende and ilmenite. The gabbro contains 40–55 vol% plagioclase, 35 vol% clinopyroxene, 5–10 vol% hornblende and apatite, with minor ilmenite (~5 vol%). The boundary between dolerite and gabbro is gradual.

The Fe ore reserve of the Cihai deposit is estimated to be more than 100 million tons, with an average tenor of 45 wt% Fe. There are many magnetite orebodies that cannot be clearly distinguished from one another but present exposure suggests the ore extends 50–500 m in length, with a width of 50–270 m and thickness of 2–52 m. In profile, orebodies occur as layers, veins and elongated lenses. Most of the magnetite ores are massive. The silicate minerals in the ore are fine-grained clinopyroxene, euhedral (10–20 μm) and equigranular (Fig. 5c, d, e and f), with minor (<vol 1%) hornblende, apatite, calcite, ilvaite and garnet. The major ore minerals in the Cihai deposit include magnetite and chalcopyrite (Fig. 5g and h), with minor ilmenite, pyrrhotite, pentlandite and pyrite (Fig. 6). Dolerite country rock is associated with all magnetite orebodies.

4. Samples and analytical methods

More than 80 samples were collected representing the different rock types from various depths in the open-pit. Altered portions of rocks and ores have been avoided during sampling. 46 samples (27 from Cihai and 19 from Cinan-) were submitted to Tianjin Geological Research Center Analytical Laboratories for mineral EPMA and LA-ICP-MS analysis after observation, description and photography.

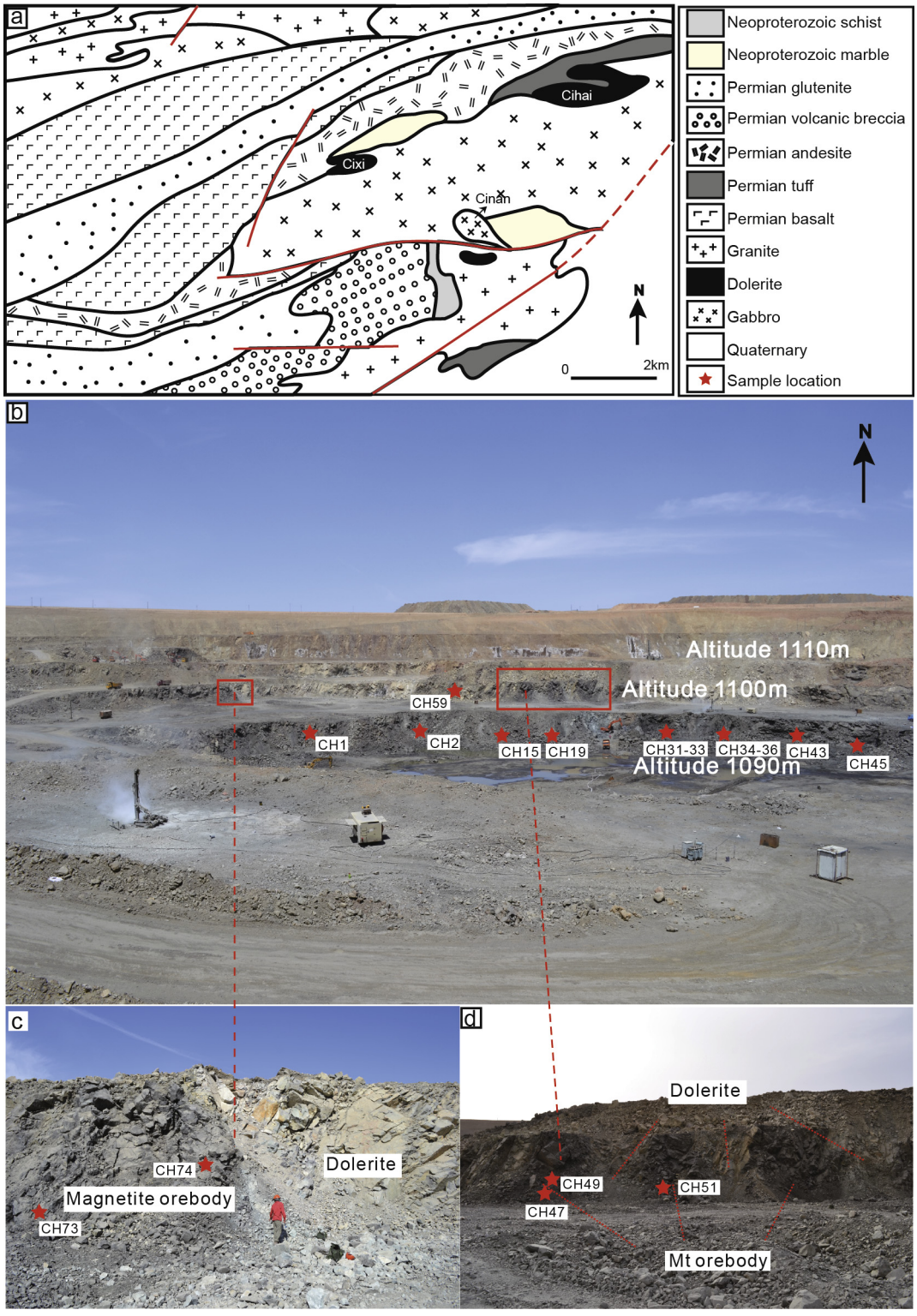

Fig. 2. (a) Simplified geologic map of Cihai region, (modified after Hou et al., 2013; and Huang et al., 2013). (b) Open pit of the Cihai Fe oxide deposit. (c and d) The contact between magnetite orebody and dolerite.

Mineral compositions were determined by wavelength dispersive spectrometry using an EPMA-1600 electron probe at Tianjin Geological Research Center, operating at an accelerating voltage of 15 kV with a 12 nA beam current, 5 μm beam, and peaking counting time of 20 s and background time of 10 s for major elements. The precision for all analyzed elements was <2.0%. Natural minerals and synthetic oxides were used as standards (the results of standards are displayed in Table 2), and a program based on the ZAF procedure was used for data reduction. Fe^{2+}–Fe^{3+} redistribution from electron microprobe analyses was carried out using the general equation of Droop (1987) for estimating Fe^{3+}. A correction was applied to magnetite and ilmenite analysis to account for the

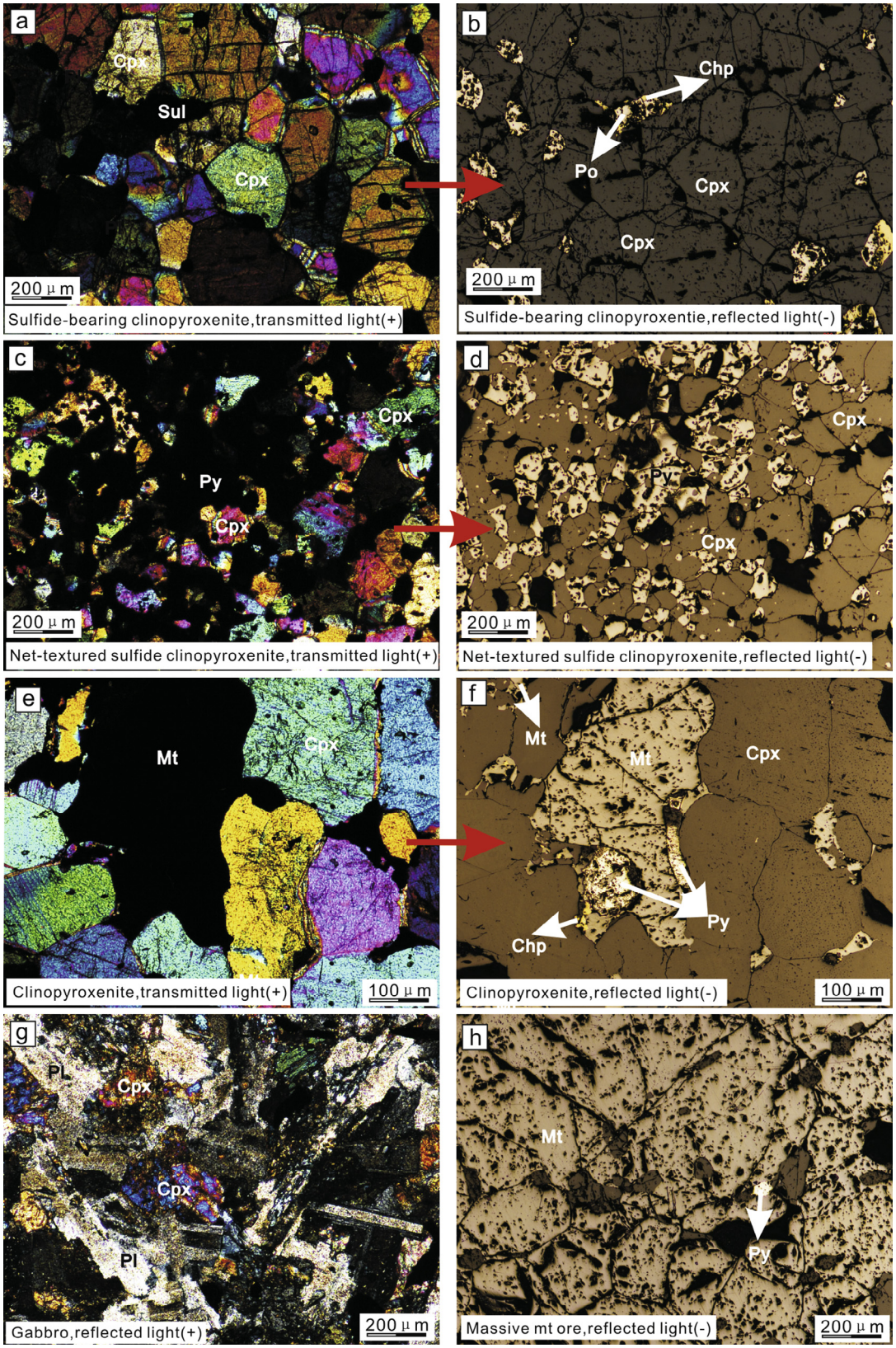

Fig. 3. Microphotographs showing the textures of major rock and magnetite ore types in the Cinan intrusion. Cpx = clinopyroxene, Pl = plagioclase, Mt = magnetite, Chp = chalcopyrite, Py = pyrite.

interference of the V $K\alpha$ and Ti $K\beta$ X-ray peaks. Representative results for each of the analyzed phases are given in Tables 3 and 4 and Appendices 1–4.

Trace elements in clinopyroxene, magnetite and apatite were determined by laser ablation inductively coupled plasma mass spectrometry (LA-ICP-MS) at the Tianjin Geological Research

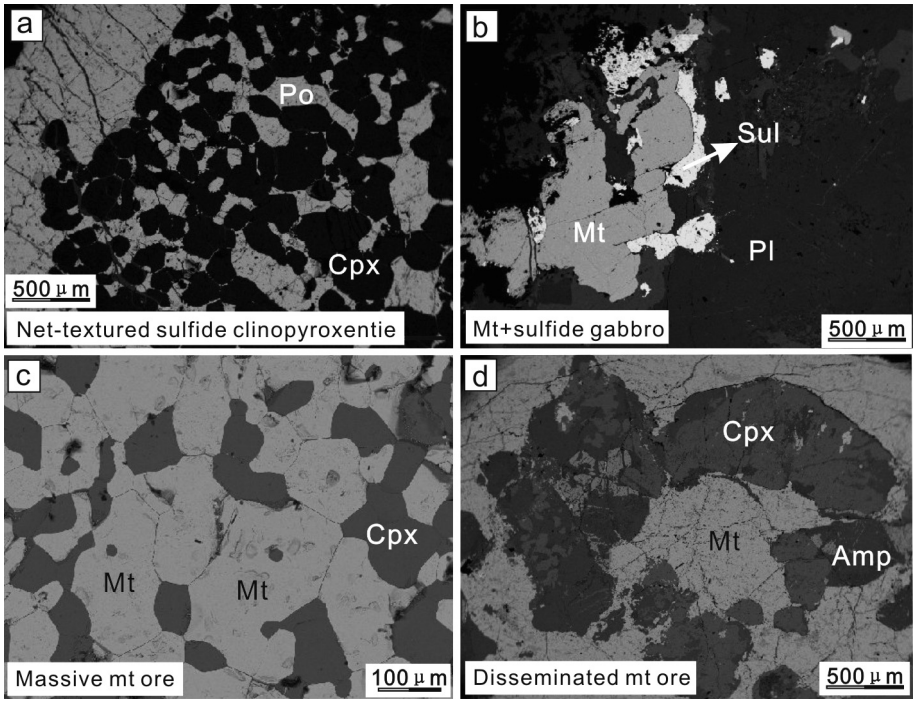

Fig. 4. Back scattered electron image of sulfide and magnetite ores from the Cinan intrusion. Cpx = clinopyroxene, Pl = plagioclase, Mt = magnetite, Chp = chalcopyrite, Py = pyrite, Sul = sulfide, Amp = amphibole.

Table 1
Age of the Cihai and Cinan mafic-ultramafic rocks and sulfide ore.

Deposit	Rock	Age	Method	References
Cihai	Diabase	268 ± 7 Ma	Whole-rock Rb-Sr isochron	Xue et al. (2000)
		263.8 ± 3.6 Ma	Zircon SHRIMP U-Pb	Qi et al. (2012)
		291.9 Ma	Zircon LA-ICP-MS U-Pb	Chen et al. (2013)
		128.5 ± 0.3 Ma	Zircon LA-ICP-MS U-Pb	Hou et al. (2013)
		275.1 ± 2.2 Ma	Zircon SIMS U-Pb	Chen et al. (2015)
	Diabase-gabbro	281.9 ± 3.2 Ma	Zircon SIMS U-Pb	Chen et al. (2015)
	Gabbro	294.8 ± 1.3 Ma	Zircon LA-ICP-MS U-Pb	Meng et al. (2014)
	Pyrite	262.3 ± 5.6 Ma	re-Os model age	Huang et al. (2013)
Cinan	Clinopyroxenite	273.6 ± 2.3 Ma	Apatite LA-ICP-MS U-Pb isochron	Chen et al. (2015)
		270.6 ± 2.1 Ma	Apatite LA-ICP-MS U-Pb concord	Chen et al. (2015)
	Gabbro	276.1 ± 0.63 Ma	Zircon LA-ICP-MS U-Pb	Meng et al. (2014)
		273.0 ± 1.9 Ma	Zircon SIMS U-Pb	Chen et al. (2015)

Center using a GeoLas 2005 coupled to an Agilent 7500a. Detailed operating conditions and data reduction methods are described in Liu et al. (2008). Helium was used as the carrier gas, with argon as the make-up gas, added to the carrier gas via a T-connector before entering the ICP-MS. Nitrogen was added into the central gas flow (Ar + He) of the Ar plasma to decrease detection limits and improve precision (Hu et al., 2008). Each analysis incorporated a background acquisition of approximately 20–30 s (gas blank) followed by 50 s of sample ablation. Elemental contents were calibrated against multiple-reference materials (BCR-2G, BIR-1G and BHVO-2G; preferred values from the GeoRem database) without applying internal standardization (Liu et al., 2008). Off-line selection and integration of background and analyte signals, time-drift correction and quantitative calibration were performed using ICPMSDataCal (Liu et al., 2008, 2010).

5. Analytical results

5.1. Clinopyroxene

Clinopyroxene is present in almost all of the lithofacies and ores of the Cihai and Cinan deposits. The major oxide and trace element compositions of clinopyroxene in the Cihai and Cinan intrusions are presented in Tables 3 and 4. Variations of major oxide contents and calculated cations are shown in Figs. 7–9.

Based on major oxide compositions, the clinopyroxene from the Cinan gabbro and clinopyroxenite varies from diopside to hedenbergite (Wo = 44–56, En = 5–47 and Fs = 7–51), whereas clinopyroxene from the Cihai gabbro and dolerite are classified as diopside (Wo = 32–52, En = 25–43 and Fs = 7–27) (Fig. 7a and b). The clinopyroxene grains from the Cinan clinopyroxenite have higher FeO and slightly lower SiO_2, MgO, CaO and TiO_2 contents than those from the gabbro (Fig. 8a, b, d and e). The clinopyroxene from the clinopyroxenite contains <0.4 wt% TiO_2 (Fig. 8e), <0.25 wt % total alkaline oxides and shows a decrease in total Fe oxide (expressed as FeO) with increasing MgO content (Fig. 8b). The clinopyroxene from the gabbro contains 0.42–1.2 wt% TiO_2 and higher total alkaline oxides (0.2–0.4 wt%). The clinopyroxene grains in the Cinan magnetitite and sulfide ore are mainly diopside (Fig. 7a), with major element compositions characterized by intermediate MgO and SiO_2 contents (between that of the Cinan clinopyroxenite and gabbro).

With the exception of CaO contents, oxides in clinopyroxene from the Cinan gabbro, massive magnetitite and sulfide ore all

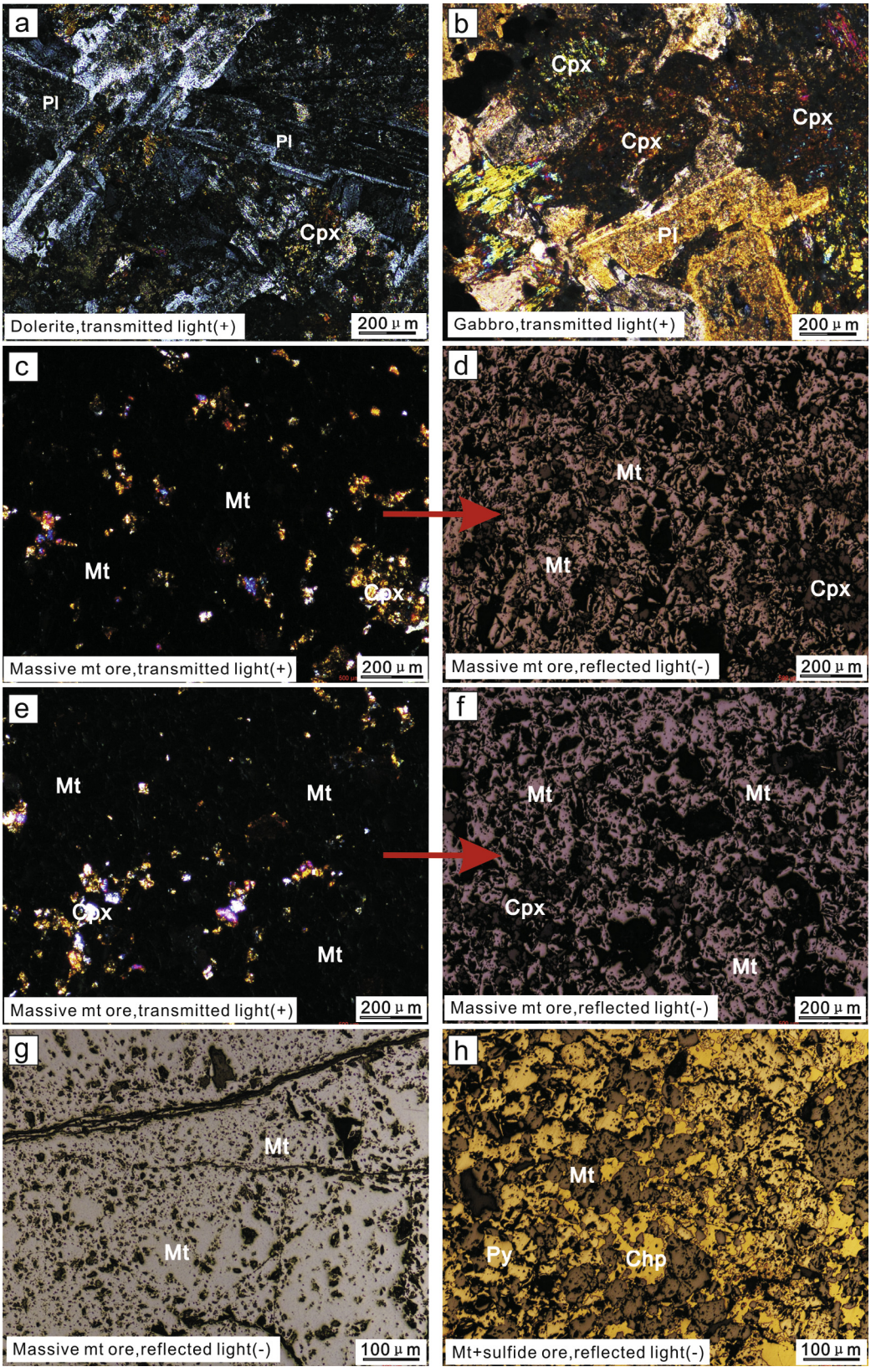

Fig. 5. Microphotographs showing the textures of major rocks and magnetite ore types in the Cihai intrusion. Cpx = clinopyroxene, Pl = plagioclase, Mt = magnetite, Chp = chalcopyrite, Py = pyrite.

correlate well with each other. Clinopyroxene from the magnetite ore contains 8.5–13.3 wt% MgO and 7.3–14.8 wt% FeO. CaO varies from 23.6 to 25.2 wt%, while the Al_2O_3 contents range from 0.01 to 1.7 wt% (Fig. 8). These clinopyroxenes have a low Cr_2O_3 content (<0.06 wt%). They also have relatively low TiO_2 (<0.1 wt%), and near-uniform Mg# (51–76, Mg# = $Mg^{2+}/(Mg^{2+} + Fe^{2+})$) relative to

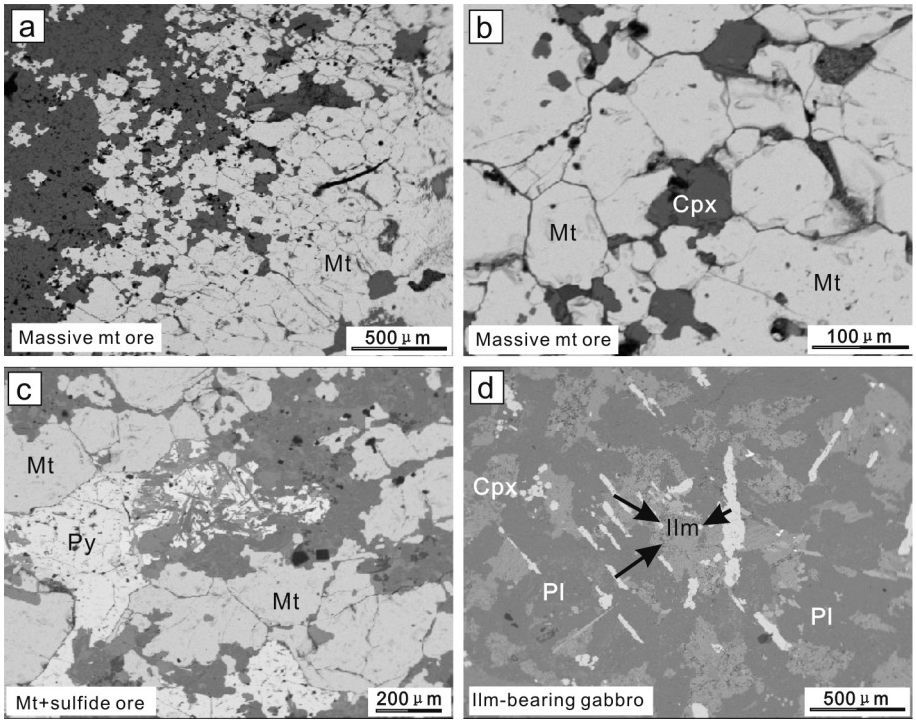

Fig. 6. Back scattered electron image of magnetite and sulfide ores from the Cihai deposit. Cpx = clinopyroxene, Pl = plagioclase, Mt = magnetite, Ilm = ilmentie, Py = pyrite.

Table 2
Oxide composition of standard.

Standard name Number	SPI-ol N = 4	SPI-bust N = 2	SPI-di N = 2	SPI-kaers N = 2	SPI-grt N = 1	JN-V N = 3	SPI-TiO_2 N = 3	SPI-Cr_2O_3 N = 1	SPI-Fe_2O_3 N = 3
SiO_2	41.75	48.74	55.52	40.24	39.53	0.25	0.12	0.08	0.06
TiO_2	0.01	0.01	0.00	4.94	0.08	0.03	98.91	0.00	0.00
Al_2O_3	0.00	0.00	0.03	12.69	22.54	0.09	0.05	0.03	0.02
Cr_2O_3	0.01	0.01	0.02	0.00	0.00	0.02	0.00	98.56	0.00
FeO	7.13	7.83	0.05	11.04	22.95	0.04	0.05	0.02	90.78
MnO	0.11	24.19	0.05	0.17	0.54	0.00	0.03	0.00	0.00
MgO	51.07	0.22	18.48	12.57	10.37	0.01	0.00	0.00	0.00
CaO	0.01	19.1	25.87	11.17	4.09	0.01	0.00	0.01	0.00
Na_2O	0.00	0.03	0.01	2.52	0.00	0.01	0.00	0.00	0.00
K_2O	0.00	0.00	0.00	1.00	0.00	0.01	0.00	0.01	0.01
NiO	0.38	0.00	0.00	0.02	0.00	0.02	0.01	0.02	0.01
V_2O_3	0.00	0.00	0.00	0.00	0.00	151.80	0.00	0.00	0.01
Total	100.46	100.15	100.03	96.33	100.1	152.28	99.16	98.72	90.91

those of the clinopyroxenite and gabbro. Clinopyroxenes in sulfide ore have a higher Al_2O_3 content (3.1–5.1 wt%) than those from the magnetite ore, clinopyroxenite and gabbro. The TiO_2 content of clinopyroxene decreases from Cinan gabbro, to sulfide ore and clinopyroxenite to magnetite ore.

The clinopyroxene from the Cihai dolerite, gabbro and magnetite ore have similar MgO (8.5–15.4 wt%), FeO (4.8–15.6 wt%), CaO (14.2–25.5 wt%), Al_2O_3 (0.05–3.9 wt%) and Cr_2O_3 contents (<0.6 wt%) (Fig. 9). However, compared to those from Cinan, the Cihai clinopyroxenes have lower Al_2O_3, TiO_2 and FeO contents and higher MgO and SiO_2 contents.

Fig. 7 provides a comparison of the clinopyroxene compositions for samples studied herein, and those previously studied in samples from the Beishan and Eastern Tianshan magmatic Cu-Ni sulfide deposits, Panxi and Xiangshanxi magnetite deposits and Tarim mafic-ultramafic intrusions and basalts. The clinopyroxene from the Beishan and Eastern Tianshan Cu-Ni deposits and the Panxi magnetite deposit all have variable but high En and Fs values (Fig. 7 a and b; Sun, 2009; Lin et al., 2011; Mao, 2014; Guo et al., 2012; Liu et al., 2012), distinct from those of the Cihai and Cinan intrusive rocks and ores. The major element geochemical features of the clinopyroxene from the Cihai dolerite, Cihai gabbro and Cinan gabbro are similar to those of the Xiangshanxi magnetite deposit and Tarim mafic-ultramafic intrusions (Jiang et al., 2004; Yang et al., 2007; Li et al., 2008b; Xiao, 2010), whereas clinopyroxene from the Cinan clinopyroxenite and the Cihai and Cinan sulfide and magnetite ores display variable and higher Fs, and lower En values than those in the dolerite and gabbro.

Clinopyroxene chondrite-normalized rare-earth element (REE) and primitive mantle-normalized trace element patterns for Cihai and Cinan mafic-ultramafic rock and ore samples are shown in Fig. 10. The primitive mantle-normalized trace element and chondrite-normalized REE patterns for clinopyroxene from the Cinan gabbro are similar to those of clinopyroxene from the Cihai gabbro and dolerite and display enrichments in large ion lithophile elements (LILE), negative high field strength element (HFSE) anomalies (Zr, Nb and Ta) and heavy rare earth element (HREE) enrichment, but no or weak negative Eu anomalies (Fig. 10).

Table 3
Average oxide compositions of clinopyroxene in the Cihai and Cinan deposits.

Deposit	Cihai				Cinan			
Rock	Dolerite	Gabbro	Fine-grained cpx-bearing massive magnetitite	Sulfide-bearing massive magnetitite	Medium-grained cpx-bearing massive magnetitite	Sparse disseminated gabbro	Gabbro	Clinopyroxenite
Number	46	26	82	17	31	10	19	105
SiO_2	52.81	53.34	52.06	51.87	51.84	49.64	52.36	48.68
TiO_2	0.07	0.07	0.02	0.04	0.03	0.59	0.75	0.14
Al_2O_3	0.41	0.50	0.86	0.88	0.64	3.99	2.35	1.96
Cr_2O_3	0.03	0.05	0.01	0.01	0.01	0.02	0.36	0.02
FeO	11.51	12.71	10.86	12.57	12.70	9.98	5.54	10.82
MnO	0.26	0.23	0.29	0.26	0.35	0.32	0.19	0.45
MgO	11.33	11.97	11.17	10.21	10.17	10.62	15.47	14.85
CaO	22.93	20.31	24.45	24.02	24.20	24.47	21.90	22.51
Na_2O	0.28	0.28	0.05	0.11	0.03	0.04	0.27	0.09
K_2O	0.01	0.04	0.01	0.00	0.00	0.00	0.01	0.00
Total	99.65	99.50	99.78	99.99	99.96	99.67	99.20	99.51
	Based on 6 Oxygen							
Si^{4+}	2.00	2.02	1.98	1.98	1.98	1.89	1.94	1.86
Ti^{4+}	0.00	0.00	0.00	0.00	0.00	0.02	0.02	0.00
Al^{IV}	0.00	-0.02	0.02	0.02	0.02	0.11	0.06	0.14
Al^{VI}	0.02	0.04	0.02	0.02	0.01	0.06	0.04	-0.05
Cr^{3+}	0.00	0.00	0.00	0.00	0.00	0.00	0.01	0.00
Fe^{2+}	0.37	0.40	0.35	0.40	0.41	0.32	0.17	0.35
Mn^{2+}	0.01	0.01	0.01	0.01	0.01	0.01	0.01	0.01
Mg^{2+}	0.64	0.68	0.63	0.58	0.58	0.60	0.85	0.85
Ca^{2+}	0.93	0.82	1.00	0.98	0.99	1.00	0.87	0.92
Na^{+}	0.02	0.02	0.00	0.01	0.00	0.00	0.02	0.01
K^{+}	0.00	0.00	0.00	0.00	0.00	0.00	0.00	0.00
Mg#	63.7	62.7	64.7	59.1	58.8	65.5	83.3	71.0
Wo	48	43	50	50	50	52	46	44
En	33	36	32	30	29	31	45	40
Fs	19	21	17	20	21	17	9	16

Clinopyroxene from the magnetite and sulfide ores have higher total trace element contents and weak negative Nb, Ta and Zr anomalies compared to gabbro (Fig. 10a), enrichment in LREE relative to HREE on chondrite-normalized plots and flat HREE patterns, with a positive or no Eu anomaly (Fig. 10b). In summary, the trace element and REEs characteristics of the clinopyroxene from the Cinan clinopyroxenite are different from those of other mafic intrusions (the Cihai and Cinan gabbro and dolerite) but similar to sulfide and magnetite ores in Cihai and Cinan. The total trace element content of Cinan clinopyroxenite clinopyroxene is lower than that in other mafic intrusive rocks and ores.

The clinopyroxene from the Cihai dolerite and gabbro has similar chondrite-normalized and primitive mantle-normalized patterns with each other, in contrast to clinopyroxene from the Cihai magnetite and sulfide ores (Fig. 10c and d). All of the clinopyroxene grains are enriched in LILE, and have negative HSFE anomalies (Zr, Nb and Ta). The chondrite-normalized REE patterns show enrichments in the LREE relative to HREE with positive Eu anomalies in the magnetite and sulfide ore samples (Fig. 10). Most of the dolerite and gabbro samples are depleted in LREE and slightly enriched in HREE, showing negative or no Eu anomalies. The magnetite and sulfide ores have lower total REE contents than those of dolerite and gabbro intrusive rocks (Fig. 10).

5.2. Magnetite

Major oxide compositions and trace element contents for magnetite from the Cinan and Cihai intrusions and ores are given in Appendices 1 and 2. *In situ* major oxide and trace element analysis was conducted on both the Cinan and Cihai massive magnetite ore and Cinan clinopyroxenite, targeting material that displayed no compositional zoning on back scattered electron (BSE) images (Figs. 4 and 6). The magnetite from the Cinan and Cihai magnetite ores show high Cr, Ni, V, Co, Ti, Mn, Ge and Sc (which substitute into magnetite) (Fig. 11g), and low Zr, Hf, Ta and Nb concentrations (incompatible in magnetite).

The calculated FeO and Fe_2O_3 contents of magnetite range from 29.5 wt% to 34.3 wt% and 52.3 wt% to 68.3 wt%, respectively, but magnetite from the Cinan clinopyroxenite shows various and higher FeO, Fe^{2+}/Fe total ratios, and lower FeO total and Fe^{3+}/Fe^{2+} ratios relative to magnetite from the iron ores (Fig. 11b). The MnO contents of magnetite from the clinopyroxenite are relatively high and restricted in range (0.1 wt% to 0.9 wt%), whereas Al_2O_3 varies from 0.6 wt% to 6.8 wt% (Fig. 11a). The magnetite ores from the Cihai and Cinan deposits show similar TiO_2, MnO and Al_2O_3 contents (0.01–0.8 wt%, 0.01–0.5 wt% and 0.01–4 wt%, respectively). The Cr, V, Ti, Ge and Ni contents in magnetite decrease from Cinan clinopyroxenite and Cinan magnetite ore to Cihai magnetite ores (Fig. 11g).

The geochemical analyses of magnetite from the iron oxide deposit related to the Emeishan mafic-ultramafic layered intrusion are also plotted in Fig. 11. These magnetite have concentration ranges and correlative trends that are similar to magnetite from the Cinan clinopyroxenite, but higher V, Ti and Cr contents than the magnetite in the Cihai and Cinan iron ore.

5.3. Apatite

Apatite is much more abundant in the dolerite, gabbro and clinopyroxenite samples. It is regarded as a magmatic phase rather than a hydrothermal mineral as it occurs as euhedral to subhedral prisms (100–200 μm) in all rocks. The compositional variability of the apatite is shown in Appendices 3 and 4.

The CaO and P_2O_5 contents of apatite are negatively correlated. The SiO_2 contents range from 0.17 wt% to 4.5 wt%, the FeO contents are generally <1 wt%. The apatite from the Cinan gabbro and clinopyroxenite has low F and high Cl contents, whereas apatite

Table 4
Average trace element contents of clinopyroxene in the Cihai and Cinan deposits.

Deposit	Cihai				Cinan		
Rock	Dolerite	Gabbro	Fine-grained cpx-bearing assive magnetitite	Sulfide-bearing massive magnetitite	Sparse disseminated gabbro	Medium-grained cpx-bearing massive magnetitite	Clinopyroxenite
Number	28	17	25	6	13	38	73
Sc	861.0	809.6	406.7	481.0	960.7	739.6	843.5
Ti	1546.6	2482.2	0.03	222.1	7036.3	2.9	748.7
V	743.1	893.7	176.1	11.5	843.3	18.3	390.1
Cr	274.6	458.0	3.3	32.6	3403.5	3.2	32.8
Co	73.8	79.4	53.7	81.4	73.7	31.6	41.0
Ni	95.7	132.6	38.4	107.6	156.8	77.2	167.0
Cu	1.6	2.4	42.2	0.4	1.2	60.0	5.9
Zn	92.7	78.4	1.0	81.9	65.5	3.8	141.5
Ga	13.3	17.0	149.5	5.5	8.8	365.4	23.0
Ge	8.8	8.0	5.0	1.8	5.8	4.8	21.1
Rb	3.2	2.3	2.0	0.2	2.2	2.5	6.0
Sr	58.5	44.3	1.1	22.1	34.5	2.6	23.1
Y	115.5	93.2	25.2	2.7	53.4	26.1	9.1
Zr	8.6	35.1	2.2	4.0	14.5	32.1	6.4
Nb	0.1	0.5	4.9	0.7	0.1	2.8	1.3
Mo	0.2	0.2	2.5	0.1	0.1	0.1	0.3
Ag	0.4	2.5	0.2	0.1	0.8	0.3	2.7
Cd	0.2	0.1	0.3	0.1	0.5	0.1	0.4
Sn	3.8	3.2	0.1	7.8	2.6	0.3	7.1
Sb	0.6	0.7	7.8	0.4	0.2	3.6	2.1
Cs	0.2	0.3	0.2	0.2	0.1	0.3	4.3
Ba	5.6	5.5	0.2	13.2	4.4	0.3	11.8
La	5.1	2.2	6.8	4.5	1.5	0.4	8.1
Ce	22.6	10.4	19.4	11.3	7.0	12.3	19.9
Pr	4.7	2.6	38.7	1.3	1.6	32.1	5.0
Nd	29.2	18.2	3.9	4.6	11.2	5.2	7.9
Sm	12.0	8.5	12.6	0.7	5.3	22.9	3.6
Eu	2.7	1.7	1.4	0.4	1.5	5.6	1.0
Gd	16.3	12.0	1.0	0.6	8.0	1.2	2.4
Tb	3.1	2.3	0.8	0.1	1.5	5.6	0.5
Dy	20.9	16.3	0.1	0.5	9.8	1.0	1.6
Ho	4.4	3.5	0.5	0.1	2.1	5.8	0.4
Er	12.4	10.4	0.1	0.3	5.7	1.2	1.1
Tm	1.8	1.6	0.2	0.04	0.8	3.1	0.2
Yb	13.2	12.4	0.03	0.3	5.0	0.5	0.9
Lu	2.2	2.2	0.2	0.07	0.7	2.8	0.2
Hf	5.7	6.7	0.04	0.3	3.1	0.4	0.8
Ta	0.01	0.04	0.4	0.04	0.0	1.2	0.2
Pb	1.4	1.3	0.1	1.4	2.0	0.1	0.6
Th	0.4	1.3	0.7	0.2	0.3	0.2	0.1
U	0.1	0.5	3.0	0.3	0.1	0.3	0.3
ΣREE	266.1	197.4	110.7	27.5	115.0	125.8	61.9

from the Cihai dolerite and gabbro has relative high F and low Cl contents (Fig. 12a and b).

Apatites from the Cinan gabbro have low LREE concentrations (mostly <9200 ppm) and total REE concentrations (2932 ppm to 9566 ppm), while those from the Cinan clinopyroxenite are generally higher in LREE (7400 ppm to 15,042 ppm) and total REE concentrations (7721 ppm to 15,436 ppm). The apatites in the Cihai dolerite and gabbro have similar total REE concentrations, between 1000 and 10,000 times chondrite values (Appendix 4, Fig. 12g and h). The REE chondrite-normalized patterns of the Cihai dolerite, gabbro and Cinan gabbro apatites show low LREE/HREE ratios and no Eu anomaly (Fig. 12g and h), while the Cinan clinopyroxenite apatites show a pronounced positive Eu anomaly and high LREE/HREE ratios (Fig. 12f).

6. Discussion

6.1. Structural setting and parental magma characteristics

Differences between parental magma types can be reflected in the Ti, Na, Si and Al composition of pyroxene (Nisbet and Pearce, 1977; Leterrier et al., 1982). In the TiO_2, Na_2O and MnO triangular diagram (Fig. 7c), diopside from the Cinan clinopyroxenite shows high TiO_2 and Na_2O contents, while clinopyroxene from the Cinan gabbro samples show TiO_2, Na_2O and MnO contents consistent with the clinopyroxene from Tarim mafic-ultramafic intrusive rock and basalts, as well as with clinopyroxene from the Panxi Fe-Ti oxide ore-related gabbro. Some clinopyroxene from Cinan sulfide-bearing samples have the same high TiO_2 content as clinopyroxene from the Panxi magnetite ore. The Panxi mafic intrusion and Fe-Ti oxide formed from highly evolved Fe-Ti-V rich ferrobasaltic magmas related to the Emeishan large igneous province (LIP) (Zhou et al., 2005; Pang et al., 2008; Wang et al., 2008). The Tarim basalts are considered to represent a LIP resulting from mantle plume activity as demonstrated by geochronologic, geophysical, tectonic and geochemical studies (Zhang et al., 2009, 2010a,b; Tian et al., 2010; Xia et al., 2012; Zhang et al., 2012; Yang et al., 2012). The equivalent-formational ages, location, and clinopyroxene major oxide characteristics implies that the Cinan mafic intrusion, iron ore and sulfide are related to tectonic activity in the Tarim LIP (Fig. 7a and c).

Clinopyroxene composition depends on primitive magma characteristics and the crystallization environment. In the spinel facies of anhydrous mantle peridotites, the most incompatible trace

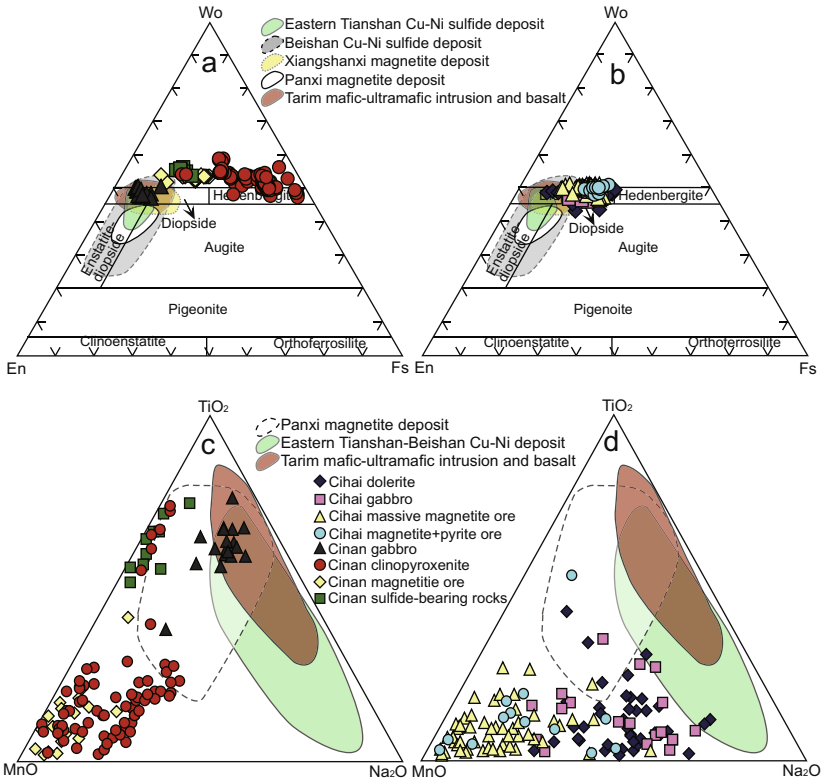

Fig. 7. Wo-En-Fs diagram of pyroxene for the Cinan (a) and Cihai (b) mafic-ultramafic intrusions (original plot after Morimoto, 1988), TiO_2-MnO-Na_2O diagram of clinopyroxene for the Cinan (c) and Cihai (d) mafic-ultramafic intrusion. The pyroxene data for the Panxi Fe deposit are from Li et al., 2010; data for the Eastern Tianshan-Beishan Cu-Ni deposit are from Sun (2009), Lin et al. (2011), Mao (2014), Guo et al. (2012) and Liu et al. (2012); data for the Xiangshanxi magnetite deposit are from Xiao (2010); data for the Tarim mafic-ultramafic intrusion and basalt are from Jiang et al. (2004), Yang et al. (2007) and Li et al. (2008b).

elements are preferentially partitioned into clinopyroxene (Hart and Dunn, 1993; Hauri et al., 1994; Witt-Eckschen and O'Neill, 2005; Claeson et al., 2007). Trace element abundance in clinopyroxene reflects the trace element content of the parental magma when the mineral grains segregated. As the incompatible element content in the residual magma increases during magma evolution and fractional crystallization, incompatible element contents in sequentially crystallized clinopyroxene increase due to the relatively stable partition coefficient between clinopyroxene and the trapped melt (Hart and Dunn, 1993; Hauri et al., 1994). The clinopyroxene chondrite-normalized REE and primitive mantle-normalized trace element patterns of the Cinan clinopyroxenite, sulfide-bearing samples and magnetite ores (Fig. 10a and b) all demonstrate similar LREE enrichment, depletion of Nb, Ta and Zr and positive Eu anomalies, suggesting that these clinopyroxenes were all derived from magma with the same trace element characteristics. However, total trace elements and REE contents increase from clinopyroxenite, through sulfide-bearing rocks to magnetite ores, implying that the crystallization order of different rocks and ores was clinopyroxenite, followed by sulfide-bearing rocks and finally, magnetitite. In contrast, the clinopyroxene from the clinopyroxenite has major oxides signatures (especially MgO) that do not suggest the above crystallization order. The earliest crystallized clinopyroxenite has clinopyroxene with the lowest MgO contents and Mg# value, but higher FeO contents. Compared to the gabbro, sulfide-bearing rocks and magnetitite, the clinopyroxenes in clinopyroxenite are characterized by slightly restricted and lower Al_2O_3 contents, lower TiO_2, CaO and SiO_2, and consistently with low trace element contents, all of which suggest uniform temperature and pressure during the early stages of magmatic evolution. The earliest crystallized clinopyroxene in the clinopyroxenite displays low MgO and SiO_2 and high FeO, suggesting that parental magma of the Cinan deposit may have been rich in FeO.

6.2. Crystallization temperature, pressure and fO_2 as recorded in the Cinan and Cihai magnetite

Magnetite is the main ore mineral in the Cinan and Cihai deposits, with magnetitite in the Cihai deposit containing a small amount of fine-grained pyroxenite (total pyroxene content <5%). Gabbro and clinopyroxenite in the Cinan deposit both contain magnetite, and the magnetite grade of the gabbro is significantly higher than that of the clinopyroxenite. Based on Fe-Ti oxide geothermometry of the silicic magma (Ghiorso and Sack, 1991), the calculated crystallization temperature of the Cinan magnetitite is 523–593 °C, and the crystallization temperature of magnetite from the Cinan clinopyroxenite is 570–598 °C. Using the same method, the crystallization temperature for the Cihai magnetite is estimated to be 463–568 °C. The reliability of the calculated temperature will be reduced when the actual fO_2 of the mineral is high, and therefore, the temperature estimates for the various rock units in the Cinan and Cihai magnetite ores and intrusion are only a relative indicator, for the purposes of discussion. The crystallization temperature of clinopyroxenite (570–598 °C) is higher than that of most magnetite ores, implying that the ultramafic phase in the Cinan deposit could represent earlier crystallization products.

Clinopyroxene major oxide contents are directly correlated with the pressure of crystallization (Brey and Kohler, 1990; Nimis and Ulmer, 1998). Using the equation reported in Nimis (1995), a more straightforward formulation that gives pressure as a function of atomic fractions based on basalt clinopyroxene is:

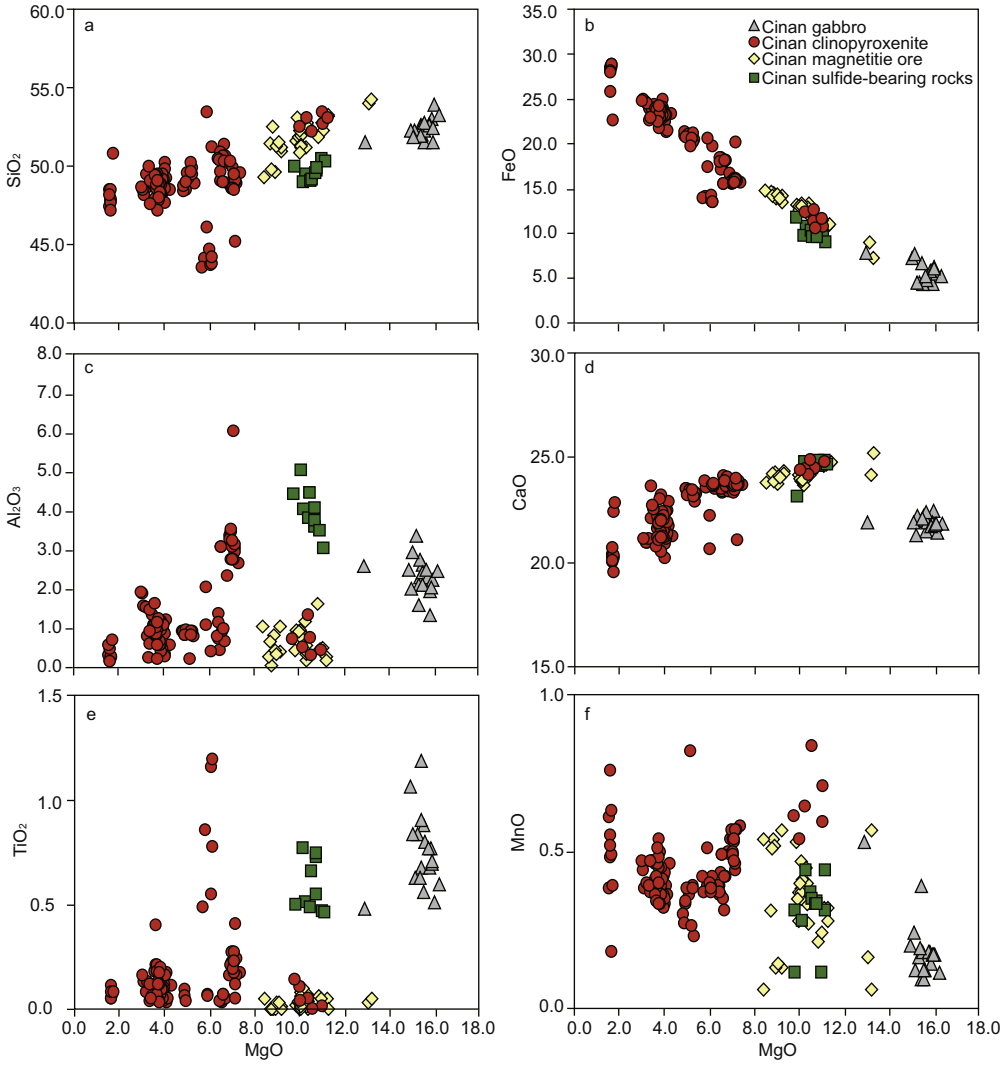

Fig. 8. Harker plots for clinopyroxene from the Cinan mafic-ultramafic intrusions and ores.

$$P(\text{kbar}) = 771.48 + 4.956 * Al_T - 28.756 * Fe^{2+}{}_{M1} - 5.345 * Fe^{3+} + 56.904 * Al_{M1} + 1.848 * Ti + 14.827 * Cr - 773.74 * Ca - 736.57 * Na - 754.81 * Mg_{M2} - 763.20 * Fe^{2+}{}_{M2} - 759.66 * Mn - 1.185(Mg_{M2})^2 - 1.876 * (Fe^{2+}_{M2})^2 \quad (1)$$

where, $(Fe^{2+}_{M1} * Mg_{M2})/(Fe^{2+}_{M2} * Mg_{M1}) = \exp(0.238 * R^{3+} + 0.289 * CNM - 2.315)$

$$CNM = Ca + Na + Mn;$$

$$R^{3+} = Al_{M1} + Fe^{3+} + Ti + Cr;$$

$$Al_{M1} = Al_{tot} - Al_T;$$

$$Al_T = (2 - Si)$$

This formula is suitable for the pressure calculations in both high and low pressure samples. The pressure of the Cinan and Cihai sulfide ores, magnetitite, clinopyroxenite and gabbro rocks according to the clinopyroxene component range from 0.10 to 0.16 kbar and 0.09 to 0.14 kbar, respectively. The pressure order of clinopyroxene (from high to low) is clinopyroxenite, sulfide-bearing rocks, gabbro and magnetitite in Cinan, and iron ores to gabbro/dolerite in Cihai.

We used the Fe^{2+}/Fe_{total} ratio of magnetite to calculate eV based on the equation of Knipping et al., 2015:

$$Fe^{2+}/Fe_{total} = 1 - 0.5879 * (C - 7111.9)^{1.2527}$$

where C is the centroid position in eV. We can then produce a redox curve according to the eV and Fe^{2+}/Fe_{total} ratio in magnetite (Fig. 11e). A correlation diagram of V versus Ni in magnetite (Fig. 11f) can be used to distinguish the fO_2 trend. V is very sensitive to the changes in oxygen fugacity as a multivalent element, and its partition coefficient between magnetite and silicate melt is mainly controlled by the oxygen fugacity (Horn et al., 1994; Canil and O'Neill, 1996; Toplis and Corgne, 2002; Mallmann and O'Neil, 2009). V is trivalent in magnetite, and the V content in magnetite will increase with decreasing oxygen fugacity, the decreasing varied V compositional range from the Cinan clinopyroxenite to Cinan magnetitite and Cihai magnetitite suggested a magmatic origin of magnetite (Fig. 11f), which strongly resembles that of the Bushveld Upper Zone, Jameson Range and Emeishan layered intrusion Fe-Ti-V deposits (Tegner et al., 2006; Pang et al., 2008; Liu et al., 2014; Karykowski et al., 2016). Furthermore, V in magnetite also heavily

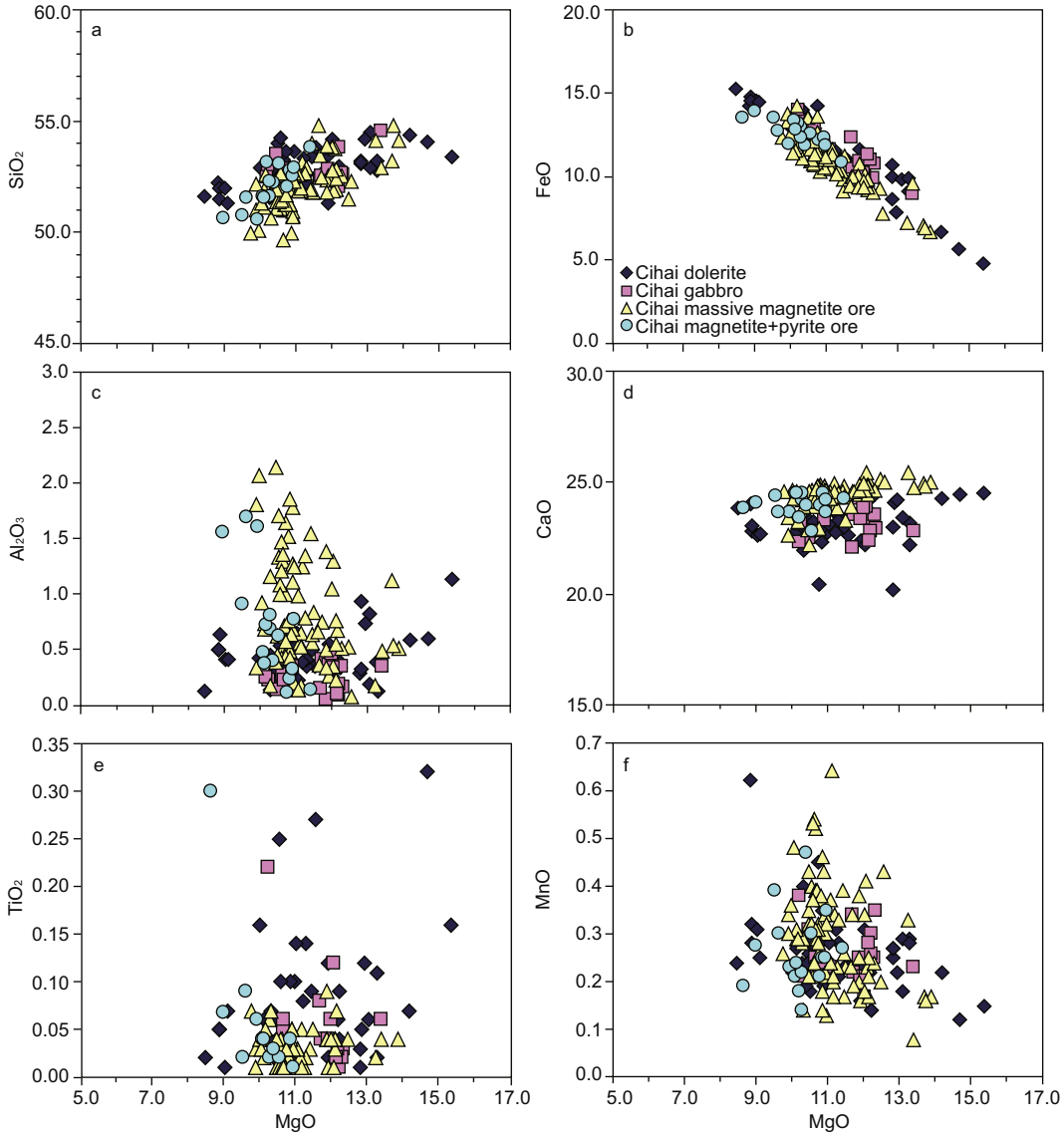

Fig. 9. Harker plots for clinopyroxene from the Cihai mafic-ultramafic intrusions and ores.

depends on the V concentrations of the parental magma. Magnetite in Jameson Range layered intrusion Fe-Ti-P-V-PGE-Au deposit has the highest V contents, suggesting the high V content in parental magma (Karykowski et al., 2016). The magnetite in the Cinan and Cihai intrusion and iron ores show normal V contents, which is much lower than Jameson Range, Bushveld layered intrusion and Emeishan layered intrusion, so we considered that the parental magma may not be rich in V. Furthermore, the V and Ti contents in magnetite from the Cihai and Cinan deposit show well linear correlation, so we propose the effect of crystallization fractionation and redox condition controlling the V content in magnetite. The Cinan clinopyroxenite magnetite signature suggests it crystallized at lower oxygen fugacity than that in Cinan and Cihai magnetitite (Fig. 11e), suggesting increasing fO_2 with magmatic evolution. This all implies that the Cinan clinopyroxenite crystallized earlier than the Cinan magnetite ores, which conforms to normal basaltic magma evolution and fractional crystallization sequences.

The occurrence, form and composition of magnetite and apatite can be used as an indicator of deposit genesis and hydrothermal function (Dare et al., 2012, 2014, 2015; Apukhtina et al., 2016). The Cinan and Cihai magnetite show no compositional zoning in BSE images (Figs. 4 and 6; distinct from typical hydrothermal magnetite), high TiO_2, Al_2O_3 and Cr_2O_3 contents, positive Zr, Hf and Sc anomalies, and low total REE contents and Ni/Cu ratios, all of which define classic magmatic magnetite. Apatite in the Cinan clinopyroxenite and gabbro exhibited high Cl and low F contents. As magma evolves from basaltic to granitic compositions, sequentially crystallized apatite will be characterized by lower Cl and higher F contents (Cherniak, 2000). Consequently, the lower Cl and higher F contents of the Cihai dolerite and gabbro suggest that they were derived from highly evolved basaltic magma. On plots of magnetite Ni/Cr ratios and apatite Sr versus Y correlations (Figs. 11d and 12d), the Cinan clinopyroxenite and gabbro plot in the area of magmatic magnetite and mafic rock related Fe ores, respectively. But the lower Ni/Cr ratios of magnetite in the Cihai massive iron ores and higher Sr and Y contents of apatite in the Cihai dolerite and gabbro imply that, after massive iron ore crystallization, gabbro and dolerite underwent hydrothermal alteration. However, the trace and rare earth element contents in apatite decrease with mineral segregation according to their compatibility in apatite (Ayers and Watson, 1993; Zirner et al., 2015; Ladenburger et al., 2016), so the higher total REE, Th and U

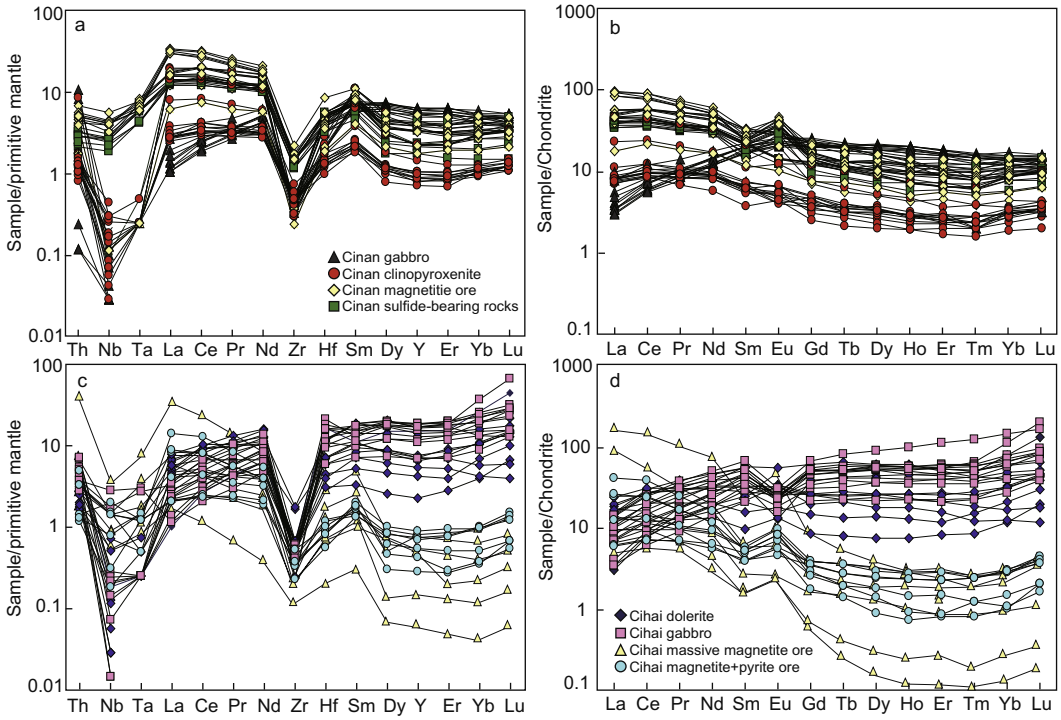

Fig. 10. Chondrite-normalized REE patterns and primitive mantle-normalized trace element patterns of the clinopyroxene from the Cinan (a and b) and Cihai (c and d) intrusive rocks. The chondrite and primitive mantle values are from Sun and McDonough (1989).

contents of the Cinan clinopyroxenite apatite (Fig. 12c and f) support the crystallization sequence suggested earlier (i.e., Cinan clinopyroxenite crystallized early). In summary, we propose that fractional crystallization was the primary process controlling magnetite and apatite composition.

6.3. Eu anomalies in clinopyroxene and apatite from the Cinan and Cihai rocks and ores

Mineral Eu anomalies are mainly controlled by three factors: magmatic characteristics, mineral crystallization order and redox conditions (Weill and Drake, 1973; Rudnick, 1992; Mazzucchelli et al., 1992; Bindeman and Davis, 2000). Mazzucchelli et al. (1992) considered that metamorphic redistribution of Eu from plagioclase could not account for positive Eu anomalies in whole rocks, clinopyroxenes and feldspar in gabbros of the deep crustal mafic intrusion of the Ivrea zone (northwestern Italy), and that the positive Eu anomaly might be related to the parent melt. There is a positive Eu anomaly in the clinopyroxene from the Cinan magnetitite and a small number of sulfide-bearing rocks, but not all of the clinopyroxenes show positive Eu anomalies (Fig. 10b). In addition, there is no significant Eu anomaly in the whole rock samples (Chen et al., 2015), suggesting that the positive Eu anomalies in clinopyroxene from the Cinan magnetitite and sulfide ores are not related to the composition of the parental magma.

Early crystallizing plagioclase preferentially incorporates Eu (Weill and Drake, 1973), leaving a Eu-depleted melt. Given that there is no Eu anomaly in the clinopyroxene from the Cinan clinopyroxenite and major sulfide-bearing rocks, large-scale plagioclase crystallization did not occur prior to clinopyroxene crystallization in those rocks and ores. The clinopyroxene in the Cinan gabbro has a completely different normalized pattern with no positive Eu anomaly and depleted LREE patterns (Fig. 10b), suggesting co-crystallization with plagioclase, consistent with the petrologic features observed in the gabbro. However, this plagioclase crystallization process did not lead to positive Eu anomalies in the clinopyroxene in magnetitite, most likely due to redox conditions. The δEu value in minerals increase with increasing oxygen fugacity (Weill and Drake, 1973). In the Cinan deposit, the oxygen fugacity was the highest when the magnetite crystallized, so the positive Eu anomalies in the clinopyroxene from the magnetite ore are higher than those in the other rocks. The same pattern can be seen in the Cihai gabbroic rocks and iron ores (Fig. 10d), Clinopyroxene in Cihai iron ores shows a significant positive Eu anomaly. Residual magma oxygen fugacity decreased, with the large amount of magnetite crystallization, so the later crystallized gabbro and dolerite clinopyroxene show strong negative Eu anomalies.

The positive Eu anomalies in clinopyroxene from the magnetite ore and magnetite + sulfide-bearing rocks from the Cinan and Cihai deposits are related directly to the oxygen fugacity. The δEu values in clinopyroxene from magnetite ore in the Cihai and Cinan deposits are high because the oxygen fugacity was high in the magma when they crystallized, while other clinopyroxene in the Cinan gabbro and clinopyroxenite with no or weakly negative Eu anomalies, can be related to the crystallization order of the clinopyroxene and plagioclase. The Cihai gabbro and dolerite clinopyroxene show pronounced negative Eu anomalies due to the sudden change in oxygen fugacity.

In the Cihai and Cinan deposits, apatite is a secondary mineral, as well as a fluid/volatile-rich mineral. In addition to the controlling factors discussed above, the Eu anomaly is also related to crystallization temperature, pressure and PH value in fluid-rich minerals. The higher the temperature and pressure and the lower PH value of the fluid/melt, the more obviously positive the apatite Eu anomaly (Sverjensky, 1984; Bau, 1991). The apatite in clinopyroxenite crystallized earlier than that in other rocks, at high pressure and temperature, resulting in the observed positive Eu anomaly. With decreasing crystallization temperature, apatite in other rocks shows no Eu anomaly.

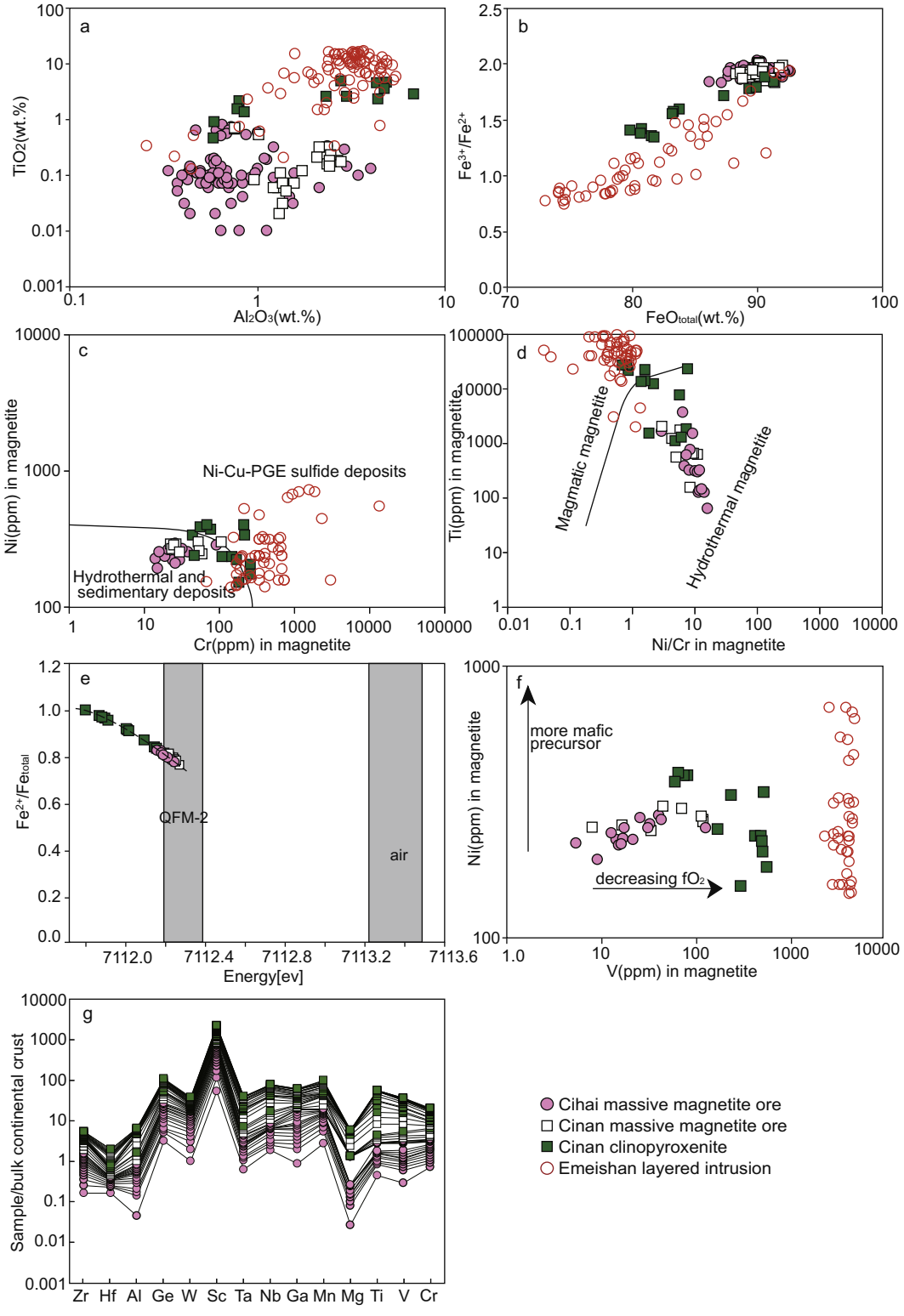

Fig. 11. Major oxide and trace element contents of magnetite (a–d, f) from the Cinan and Cihai deposits. Calculated energy (eV) versus Fe^{2+}/Fe_{total} for magnetite (e); Bulk continental crust-normalized multi-element variation diagrams of lithophile element concentrations in magnetite from Cinan and Cihai (g). The bulk continental crust values are from Rudnick and Gao (2003). The dividing line in (c) and (d) is from Dare et al. (2014). The trend line in (f) is from Chen et al. (2015) (e) was modified from Knipping et al. (2015). Date for Emeishan layer intrusions are from Pang et al. (2008) and Liu et al. (2014).

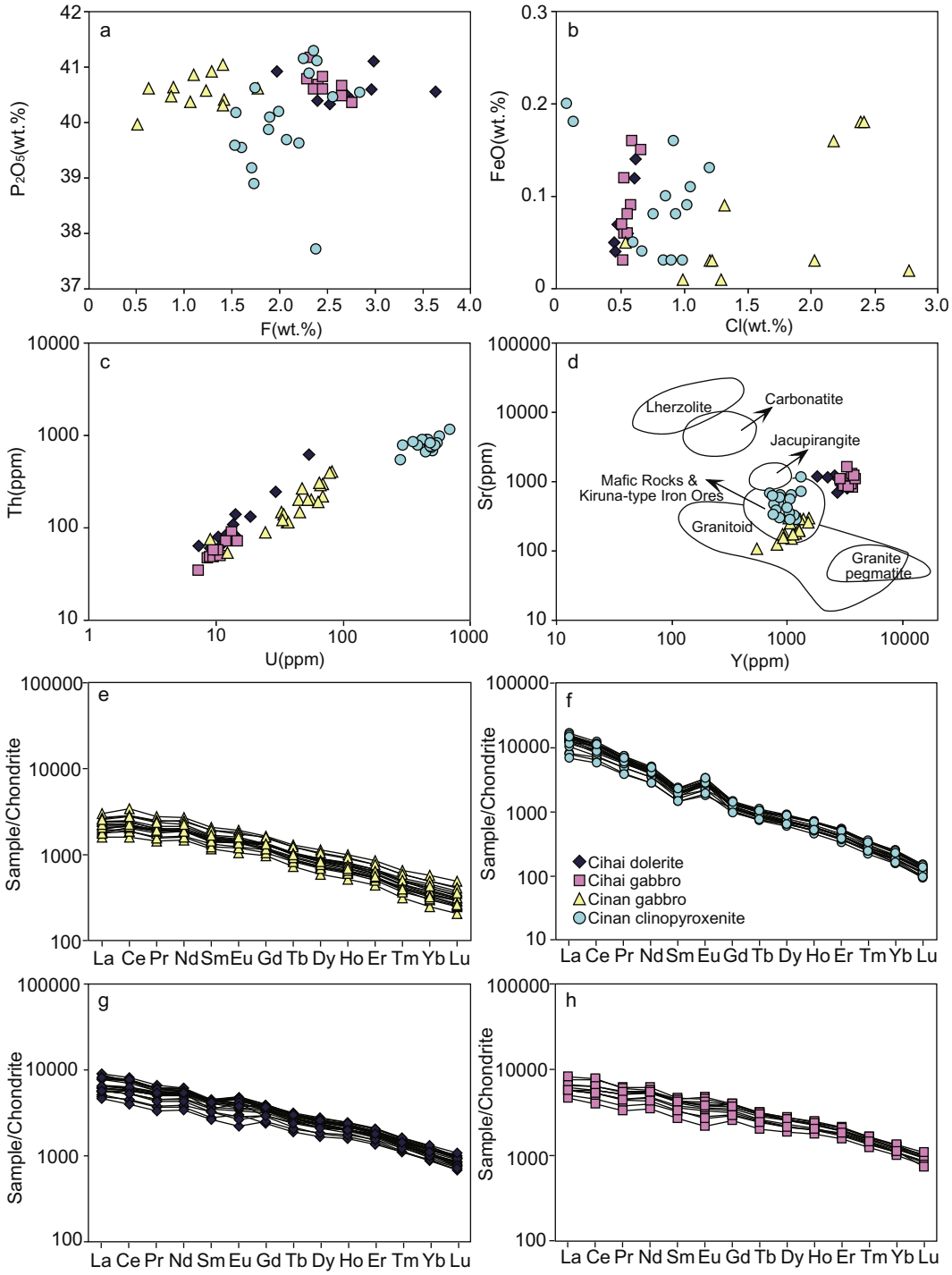

Fig. 12. Major oxide and trace elements concentrations in apatite from the Cinan and Cihai intrusions (original plot from Belousova et al., 2002) Chondrite-normalized REE patterns for apatite from Cinan (a–d) and Cihai intrusive rocks (e–h). The chondrite values and the primitive mantle values are from Sun and McDonough (1989).

6.4. Fractional crystallization at the Cinan and Cihai deposits

6.4.1. Mineral crystallization sequence at the Cinan deposit

The partition coefficients for major oxides between sulfides, silicate minerals, oxides and melt are relatively stable (Peach and Mathez, 1993). In addition to, the Fe, Ni and other elements exchange reaction between silicate and sulfide minerals requires restrictive conditions (Hirschmann and Ghiorso, 1994; Li et al., 2001). Furthermore, while Na, Ti and V diffusion/reequilibration rates in olivine are fast (Qian et al., 2010), the same cannot be said for clinopyroxene. We chose unaltered clinopyroxene in fresh samples for *in situ* major oxide and trace element analysis and placed the analysis spots in the core of the grain to minimize the impact of diffusion and alteration. For these reasons we consider that reequilibration/diffusion and alteration are not major controls on the clinopyroxene major element composition and we focused on the effects of fractional crystallization.

The clinopyroxene in the Cinan sulfide-bearing rocks has higher MgO, Al_2O_3 and TiO_2 contents, and lower FeO contents than the clinopyroxene in the Cinan magnetite ores (Fig. 8). This suggests

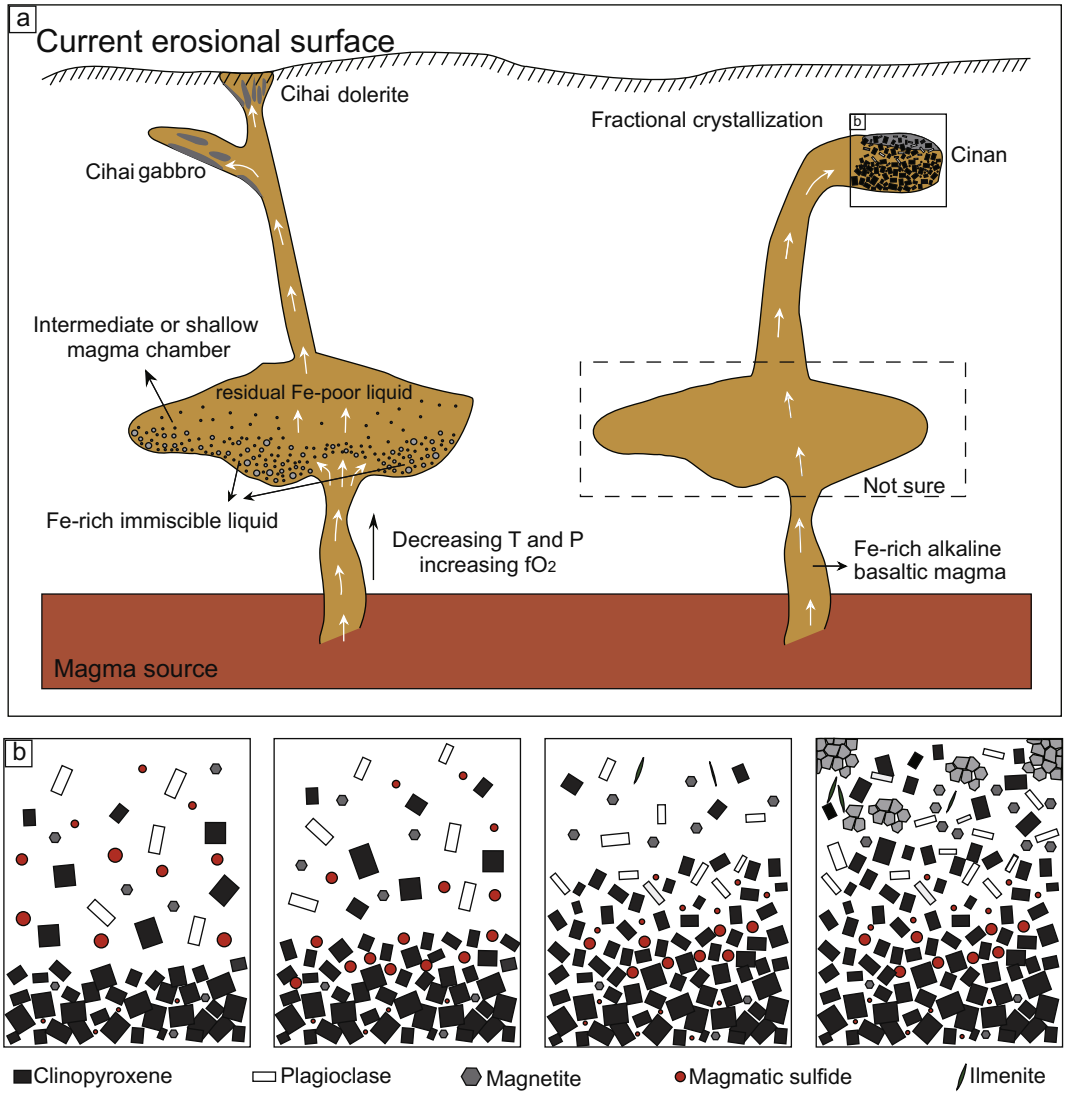

Fig. 13. Model of magma evolution and formation of magnetite ores in the Cihai and Cinan intrusion. (a). The basaltic magma was emplaced at depth, with magnetite segregation (and formation of the Cinan magnetite ores) occurring in relatively low fO_2 conditions, after clinopyroxenite and gabbro fractional crystallization. The evolved Fe-rich basaltic magma rapidly rose to lower crustal levels, forming an immiscible Fe-Ti oxide magma and leaving a Fe-poor residual magma as fO_2 increased and temperature and pressure decreased. These magmas were emplaced at different levels in the crust, forming the Cihai gabbro and dolerite, respectively. Finally, an immiscible Fe-Ti oxide magma was emplaced into the earlier formed dolerite, resulting in a distinct boundary between the magnetite ores and dolerite. (b). Graphic representation of the crystallization sequence at the Cinan deposit where the order of crystallization was clinopyroxenite-sulfide-gabbro-magnetite ore.

that the sulfide-bearing rocks crystallized earlier from the magma than the Cinan magnetite ores, which is consistent with the calculated pressures. The low TiO_2 contents in clinopyroxene from the Cinan magnetite ores is likely due to the preferential incorporation of Ti into co-precipitated magnetite.

The Al_2O_3 and TiO_2 contents of clinopyroxene in the Cinan gabbro are intermediate between that of sulfide-bearing rocks and magnetite ores (Fig. 8), indicating that the pressure and crystallization time of the gabbro were interposed between the sulfide-bearing rocks and magnetite ores. The clinopyroxene crystallization sequence at the Cinan deposit can, therefore, be interpreted as clinopyroxenite, followed by sulfide-bearing rocks, gabbro and magnetite ore. However, the clinopyroxene from the Cinan clinopyroxenite can be classified as diopside and hedenbergite. Diopside has high MgO and Al_2O_3 contents, and low FeO and TiO_2 contents, while hedenbergite has low MgO and Al_2O_3 contents, and high FeO and MnO contents. Both types of clinopyroxene in Cinan display uniform trace element and REE patterns, indicating that they crystallized from the same magma. Assuming that oxide element analysis indicates crystallization at different degrees of evolution, the diopside must be the earlier crystallizing phase.

6.4.2. Mineral crystallization sequence at the Cihai deposit

All of the clinopyroxene in the Cihai intrusive rocks and ores is diopside. The LREE enrichment, depleted Nb, Ta and Zr, high Al_2O_3, and low TiO_2 and total REE contents in the clinopyroxene from the Cihai magnetite ores suggest that these grains crystallized before plagioclase. On the other hand, the HREE enrichment, negative Eu anomalies and low Al_2O_3 contents of the clinopyroxene from the Cihai gabbro and dolerite, indicate that the clinopyroxene crystallized significantly later than the clinopyroxene in magnetite ores. All of the lithophile elements (Cr, Ti, V, Al, Mn, Sc, Nb, Ga, Ge, Ta, Hf, W and Zr) are compatible in Fe oxide, and concentrations of these elements are highest in the early-forming Fe oxide (Dare et al., 2012). This might be the key reason for the varied trace element contents, low TiO_2 and higher LREE/HREE ratios in the clinopyroxene from the magnetite ores in the Cihai deposit. Accordingly, we propose that clinopyroxene in magnetite ores

are the earliest crystallizing phase in the Cihai deposit. Based on the similar fO_2, clinopyroxene content and pressure, we cannot discern the crystallization order between gabbro and dolerite in the Cihai deposit.

6.5. Mineralization mechanisms and relationship between the Cinan and Cihai deposits

The Cinan and Cihai parental magmas were derived from the similar mantle source. Low oxygen fugacity magnetite in clinopyroxenite, early sulfide segregation, accompanied by the high FeO and Al_2O_3 contents clinopyroxene, both proved the parental magma was Fe-rich and partially reduced. The similarity in V, Ti, Cr and Ni/Cr ratios between the Cinan magnetite and typical magmatic genesis in the Emeishan layered intrusion iron oxide ores, further argue for magmatic genesis for the Cinan iron ore. Several lines of evidence suggest that the earliest crystallized phase in the Cinan deposit was clinopyroxenite, such as the high Al_2O_3 contents, low SiO_2 and total REE contents, and lack of Eu anomaly in clinopyroxene. Magnetite crystallized during the late stages of magma evolution as fO_2 and Fe content increased, and fractional crystallization was the key factor controlling Cinan iron ore mineralization. The sulfide and Fe oxide ores originated from Fe-rich basaltic parental magma, where sulfur saturation and sulfide segregation occurred first due to Fe-rich clinopyroxene crystallization, followed by gabbro crystallization. Finally, the increasing fO_2 and FeO contents of the residual magma, led to magnetite segregation (Fig. 13b).

The density of Fe-Ti oxide (4.5–4.6g/cm^3) is greater than that of basaltic magma (3.1–3.2 g/cm^3) (Emmons, 1904; Charlier et al., 2006), and the liquidus temperature of Fe-Ti oxide is 1400 °C, so at high oxygen fugacity, Fe-Ti oxides segregate early from Fe-rich magma (Taylor, 1963). The fine-grained clinopyroxene-bearing magnetite ore was the earliest crystallized rock in the Cihai deposit. Moreover, magnetite from the fine-grained clinopyroxene-bearing iron ores shows typical characteristics of magmatic genesis. Accordingly, it is proposed that, in the deeper portions of the Cihai district, there was an intermediate or shallow magma chamber that, with decreasing temperature and pressure, formed a denser Fe-rich immiscible liquid and residual Fe-poor liquid. The relatively depleted residual liquid, at the top of the magma chamber, ascended and was emplaced at shallow upper crustal levels, and formed gabbro, then magma was continually emplaced along the fault and formed sub-volcanic dolerite. This is consistent with dolerite and gabbro zircon U-Pb crystallization ages of 275.1 ± 2.2 Ma and 281.9 ± 3.2 Ma, respectively (Chen et al., 2015), and the compositional characteristics of the clinopyroxene from the Cihai gabbro described earlier (low total REE and FeO contents, high MgO contents, and negative Eu anomalies). The Fe-rich immiscible liquid was emplaced into the former dolerite and gabbro along the magma channel and formed magnetite ore (Fig. 13a). The dolerite and gabbro experienced alteration during the emplacement and mineralization of magnetite. The pivotal mineralization mechanism responsible for the formation of magnetite ores at Cihai was formation of an immiscible Fe-rich melt at high fO_2, during the early stages of magma evolution.

The Cihai and Cinan deposits are both Fe oxide deposits, inherently suggesting relatively oxidized conditions. The whole rock major and trace element geochemical characteristics of the Cinan clinopyroxenite and gabbro imply that crustal contamination function was weak (Chen et al., 2015). While $\delta^{34}S$ values of three sulfide minerals (pyrrhotite, chalcopyrite and pyrite) are characteristic of S derived from mantle (Xue et al., 2000). Oxidized conditions, limited crustal contamination and lack of crustal S signatures are not conducive to magmatic Cu-Ni sulfide deposit formation. S solubility heavily depends on the Fe activity of the magma and in most magnetitite-hosted PGE-(Cu) reefs, S saturation is believed to be reached in response to the segregation of magnetite, leading to a drop in iron activity (Karykowski et al., 2016). Nevertheless, magnetite crystallized after sulfide minerals in the Cinan deposit, so the most probable reason for the presence of small amounts of sulfides in the Cinan deposit was Fe-rich clinopyroxene fractional crystallization, leading to a decrease in the residual magma Fe content and a reduction in iron activity. However, magma evolution and the differentiation of Fe-rich clinopyroxene alone did not trigger large-scale S saturation and the Cinan iron deposit did not form an independent, economic-grade Cu-Ni sulfide deposit.

7. Conclusions

The clinopyroxene in the Cinan clinopyroxenite is FeO-rich and Si and Ti-poor, consistent with the clinopyroxene component of large-scale Cu-Ni sulfide deposits in the Eastern Tianshan and Panxi areas, as well as Tarim mafic intrusion and basalt, implying the Cinan mafic intrusion and sulfide is related to tectonic activity in the Tarim LIP. This also suggests a Fe-rich basaltic magma. The similar clinopyroxene, apatite and magnetite chemical features between the Cihai and Cinan gabbro (e.g., depleted LREE, negative Zr, Hf, Nb and Ta, anomalies in clinopyroxene, lack of Eu anomalies in apatite and similar oxygen fugacity), illustrate that they originated from the same magmatic source. The parental magmas for the Cinan and Cihai deposits evolved separately and were emplaced into different parts of the upper crust. Basaltic magma evolution and emplacement was deeper, where magnetite segregated and formed the Cinan disseminated magnetite ores in low fO_2 conditions after clinopyroxenite and gabbro fractional crystallization. The evolved Fe-rich basaltic magma rose to shallow crustal levels rapidly, forming a denser immiscible Fe-Ti oxide magma and residual Fe-poor magma with increasing fO_2. Both magmas were emplaced at different crustal depths, and formed the Cihai magnetitite, dolerite and gabbro, respectively. Firstly, the Fe-poor magma was emplaced, and formed dolerite and gabbro. Then immiscible Fe-Ti oxide magma was emplaced into the earlier formed dolerite because of uplift of a late magma pulse and the boundary between magnetitite and dolerite is distinct.

Acknowledgments

We are grateful to Guang-Ming Li for advice on regional geology. This study was financially supported by the Nature Science Foundation of China (No. 41472075) for Dr. Dong-Mei Tang and National Geological Survey Project of Altay and Junggar (No. DD2016006). We are very grateful for two excellent reviews, which greatly improved the manuscript.

Appendix A. Supplementary data

Supplementary data associated with this article can be found, in the online version, at http://dx.doi.org/10.1016/j.oregeorev.2017.01.019.

References

Apukhtina, O.B., Kamenetsky, V.S., Ehrig, K., Kamenetsky, M.B., McPhie, J., Maas, R., Meffre, S., Goemann, K., Rodemann, T., Cook, N.J., Ciobanu, C.L., 2016. Postmagmatic magnetite- apatite assemblage in mafic intrusions: a case study of dolerite at Olumpic Dam, South Australia. Contrib. Mineral. Petrol. http://dx.doi.org/10.1007/s00410-015-1215-7.

Ashwal, L., 1993. Anorthosites. Springer, Heidebleg.

Ayers, J.C., Watson, E.B., 1993. Apatite/fluid partitioning of rare earth elements and strontium: Experimental results at 1.0 GPa and 1000°C and application to models of fluid-rock interaction. Chem. Geol. 110, 299–314.

Bau, M., 1991. Rare-earth element mobility during hydrothermal and metamorphic fluid-rock interaction and the significance of the oxidation state of europium. Chem. Geol. 93, 219–230.
Belousova, E.A., Griffin, W.L., O'Reilly, S.Y., Fisher, N.I., 2002. Apatite as an indicator mineral for mineral exploration: trace-element compositions and their relationship to host rock type. J. Geochem. Explor. 76, 45–69.
Bindeman, I.N., Davis, A.M., 2000. Trace element partitioning between plagioclase and melt: Investigation of dopant influence on partition behavior. Geochim. Cosmochim. Acta 64, 2863–2878.
Bonnetti, C., Cuney, M., Michels, R., Truche, L., Malartre, F., Liu, X.D., Yang, J.X., 2015. The multiple roles of sulfate-reducing bacteria and Fe-Ti oxides in the genesis of the Bayinwula Roll front-type uranium deposit, Erlian Basin, NE China. Econ. Geol. 110, 1059–1081.
Brey, G.P., Kohler, T., 1990. Geothermometry in four-phase lherzolites. II. New thermobarometers, and practical assessment of existing thermobarometers. J. Petrol. 31, 1353–1378.
Canil, D., O'Neill, H.C., 1996. Distribution of ferric iron in some upper-mantle assemblages. J. Petrol. 37, 609–635.
Cao, J., Wang, Y., Xing, C.M., Xu, Y.G., 2014. Origin of the early Permian Wajilitag igneous complex and associated Fe-Ti oxide mineralization in the Tarim large igneous province, NW China. J. Asian Earth Sci. 84, 51–68.
Cawthorn, R.G., McCarthy, T.S., 1980. Variations in Cr content of magnetite from the upper zone of the Bushveld Complex – evidence for heterogeneity and convection currents in magma chambers. Earth Planet. Sci. Lett. 46, 335–343.
Charlier, B., Grove, T., 2012. Experiments on liquid immiscibility along tholeiitic liquid lines of descent. Contrib. Mineral. Petrol. 164, 27–44.
Charlier, B., Duchesne, J.C., Vander, A., 2006. Magma chamber processes in the Tellnes ilmenite deposit (Rogaland Anorthosite Province, SW Norway)and the formation of Fe-Ti ores in massif-type anorthosites. Chem. Geol. 234, 264–290.
Chen, B., Qin, K.Z., Tang, D.M., Mao, Y.J., Feng, H.Y., Xue, S.C., Yao, Z.S., 2015. Lithological, chronological and geochemical characteristics of Cihai iron deposit, Eastern Xinjiang: Constraints on genesis of mafic-ultramafic and syenite intrusions and mineralization. Acta Petrol. Sin. 31 (8), 2156–2174 (In Chinese with English abstract).
Chen, J.P., Liao, Q.A., Luo, T., Zhang, X.H., Guo, D.B., Zhu, H.L., Liu, X.M., 2013. Zircon U–Pb geochronology and genesis study on the mafic complex from diabase-type iron deposit in Cihai, Beishan area. Geol. Science Tech. Infor. 32 (4), 76–83 (In Chinese with English abstract).
Cherniak, D.J., 2000. Rare earth element diffusion in apatite. Geochim. Cosmochim. Acta 64, 3871–3885.
Claeson, D.T., Meurer, W.P., Hogmalm, K.J., Larson, S.A., 2007. Using LA-ICPMS mapping and sector zonation to understand growth and trace-element partitioning in sector-zoned clinopyroxene Oikocrysts from the Norra Ulvo gabbro, Sweden. J. Petrol. 48 (4), 711–728.
Dare, S.A.S., Barnes, S.J., Beaudion, G., 2012. Variation in trace element content of magnetite crystallizaed from a fractionating sulfide liquid, Sudbury, Canada: Implications for provenance discrimination. Geochim. Cosmochim. Acta 88, 27–50.
Dare, S.A.S., Barnes, S.J., Beaudoin, G., Meric, J., Boutroy, E., Potvin-Doucet, C., 2014. Trace elements in magnetite as perogenetic indicators. Miner. Deposita 49, 785–796.
Dare, S.A.S., Barnes, S.J., Beaudoin, G., 2015. Did the massive magnetite "lava flows" of El Laco (Chile) form by magmatic or hydrothermal processes? New constraints from magnetite composition by LA-IC-MS. Miner. Deposita 50, 607–617.
Downes, H., Reichow, M.K., Mason, P.R.D., Beard, A.D., Thirlwal, M.F., 2003. Mantle domains in the lithosphere beneath the French Massif Central: Trace element and isotopic evidence from mantle clinopyroxenes. Chem. Geol. 200, 71–87.
Driouch, Y., Beziat, D., Gregoire, M., Laguenini, F., Abbou, B.M., Ntarmouchant, A., Roddza, M., Dahire, M., Bennouna, A., Belkasmi, M., Brusset, S., Debat, P., 2010. Clinopyroxene trace element compositions of cumulate mafic rocks and basalts from the Hercynian Moroccan Central Meseta: Petrogenetic implications. J. African Earth Sci. 56, 97–106.
Droop, G.T.R., 1987. A general equation for estimating Fe^{3+} concentrations in ferromagnesian silicates and oxides from microprobe analyses, using stoichiometric criteria. Mineral. Mag. 51, 431–436.
Duchesne, J.C., 1999. Fe-Ti deposits in Rogaland anorthosites (South Norway): geochemical characteristics and problems of interpretation. Miner. Deposita 34 (2), 182–198.
Emmons, S.F., 1904. Theories of ore deposition historically considered. Geol. Soc. Am. Bull. 15, 12.
Gao, J., Li, M.S., Xiao, X.C., Tang, Y.Q., He, G.Q., 1998. Paleozoic tectonic evolution of the Tianshan orogen, northwestern China. Tectonophysics 287, 213–231.
Gao, J., Long, L.L., Qian, Q., Huang, D.Z., Su, W., Klemd, R., 2006. South Tianshan: a late Paleozoic or a Triassic orogen. Acta Petrol. Sin. 22, 1049–1061 (in Chinese with English abstract).
Gao, J., Long, L.L., Klemd, R., Qian, Q., Liu, D.Y., Xiong, X.M., Su, W., Liu, W., Wang, Y. T., Yang, F.Q., 2009. Tectonic evolution of the South Tianshan orogen and adjacent regions, NW China: geochemical and age constraints of granitoid rocks. Int. J. Earth Sci. 98, 1221–1238.
Ghiorso, M.S., Sack, O., 1991. Fe-Ti oxide geothermometry: thermodynamic formulation and the estimation of intensive variables in silicic magmas. Contrib. Mineral. Petrol. 108, 485–510.
Guo, X.N., Jiang, C.Y., Song, Y.F., Xia, M.Z., Ling, J.L., Xia, Z.D., Wang, B.Y., 2012. Petrogenesis of the olivine gabbronorite in Pobei complex, Northeast Tarim plate. Geol. Rev. 58 (5), 873–886 (in Chinese with English abstract).
Harney, D.M.W., Merkle, R.K.W., von Gruenewaldt, G., 1990. Platinum-group element behavior in the lower part of the Upper Zone, Eastern Bushveld Complex-implications for the formation of the main magnetite layer. Econ. Geol. 85, 1777–1789.
Hart, S.R., Dunn, T., 1993. Experimental cpx/melt partitioning of 24 trace elements. Contrib. Mineral. Petrol. 113, 1–8.
Hauri, Erik H., Wagner, T.P., Grove, T.L., 1994. Experimental and natural partitioning of Th, U, Pb and other trace elements between garnet, clinopyroxene and basaltic melts. Chem. Geol. 117, 149–166.
Hirschmann, M., Ghiorso, M.S., 1994. Activities of nickel, cobalt, and manganese silicates in magmatic liquids and applications to olivine/liquid and silicate/metal partitioning. Geochim. Cosmochim. Acta 58, 743–770.
Horn, I., Foley, S.F., Jackson, S.E., Jenner, G.A., 1994. Experimentally determined partitioning of high field strength- and selected transition elements between spinel and basaltic melt. Chem. Geol. 117 (1–4), 193–218.
Hou, T., Zhang, Z.C., Santosh, M., Encarnacion, J., Wang, M., 2013. The Cihai diabase in the Beishan region, NW China: Isotope geochronology, geochemistry and implications for Cornwall-style iron mineralization. J. Asian Earth Sci. 70–71, 231–249.
Hu, Z.C., Gao, S., Liu, Y.S., Hu, S.H., Chen, H.H., Yuan, H.L., 2008. Signal enhancement in laser ablation ICP-MS by addition of nirogen in the central channel gas. J. Anal. At. Spectrom. 23, 1093–1101.
Huang, X.W., Zhou, M.F., Qi, L., Gao, J.F., Wang, Y.W., 2013. Re–Os isotopic ages of pyrite and chemical composition of magnetite from the Cihai magmatic–hydrothermal Fe deposit, NW China. Miner. Deposita 48, 925–946.
Jahn, B.M., Windley, B., Natal'in, B., Dobretsov, N., 2004. Phanerozoic continental growth in Central Asia. J. Asian Earth Sci. 23, 599–603.
Jiang, C.Y., Zhang, P.B., Lu, D.R., Bai, K.Y., 2004. Petrogenesis and magma source of the ultramafic rocks at Wajilitage region, western Tarim plate in Xinjiang. Acta Petrol. Sin. 20 (6), 1433–1444 (In Chinese with English abstract).
Jiang, C.Y., Cheng, S.L., Ye, S.F., Xia, M.Z., Jiang, H.B., Dai, Y.C., 2006. Lithogeochemistry and petrogenesis of Zhongposhanbei mafic rock body, at Beishan region, Xinjiang. Acta Petrol. Sin. 22 (1), 115–126 (in Chinese with English abstract).
Karkkainen, N., Appelqvist, H., 1999. Genesis of a low-grade apatite-ilmenite-magnetite deposit in the Kauhajarvi gabbro, west Finlan. Mineral. Deposita 34, 754–769.
Karykowski, B.T., Polito, P.A., Maier, W.D., Gutzmer, J., Krause, J., 2016. New insights into the petrogenesis of the Jameson Range layered intrusion and associated Fe-Ti-V-PGE-Au mineralization, West Musgrave Province, Western Australia. Miner. Deposita. http://dx.doi.org/10.1007/s00126-016-0655-y.
Kerr, A., Ryan, B., 2000. Threading the eye of the needle: lessons form the search for another Voisey's Bay in Labrador, Canada. Econ. Geol. 95 (4), 725–748.
Klemm, D.D., Henckel, J., Dehm, R., Gruenewaldt, G., 1985. The geochemistry of titanomagnetite in magnetite layers and their host rocks of the eastern, Bushveld Complex. Econ. Geol. 89, 1075–1088.
Knipping, J.L., Behrens, H., Wilke, M., Gottlicher, J., Stabile, P., 2015. Effect of oxygen fugacity on the coordination and oxidation state of iron in alkali bearing silicate melts. Chem. Geol. 411, 143–154.
Kushiro, I., 1960. Si-Al relation in clinopyroxenes from igneous rocks. Am. J. Sci. 258, 548–554.
Ladenburger, S., Marks, M.A.W., Upton, B., Hill, P., Wenzel, T., Markl, G., 2016. Compositional variation of apatite from rift-related alkaline igneous rocks of the Gardar Province, South Greenland. Am. Mineral. 101, 612–616.
Lee, C.A., 1996. A review of mineralization in the Bushveld Complex and some other layered intrusions. In: Cawthorn, R.G. (Ed.), Layered Intrusions. Elsevier, Amsterdam, pp. 103–145.
Lester, G.W., Clark, A.H., Kyser, T.K., Naslund, H.R., 2013. Experiments on liquid immiscibility in silicate melts with H_2O, P, S, F and Cl: implications for natural magmas. Contrib. Mineral. Petrol. 166, 329–349.
Leterrier, J., Maury, R.C., Thonon, P., Girard, D., Marchal, M., 1982. Clinopyroxene composition as a method of identification of the magmatic affinities of paleovolcanic series. Earth Planet. Sci. Lett. 59, 139–154.
Li, Z.L., Yang, S.F., Chen, H.L., Langmuir, C.H., Yu, X., Lin, X.B., Li, Y.Q., 2008b. Chronology and geochemistry of Taxinan basalts from the Tarim basin: evidence fro Permian plume magmatism. Acta Petrol. Sin. 24 (5), 959–970 (In Chinese with English abstract).
Li, Z.R., Zhang, Y., Li, G., 2008a. Reserves verification report about the Cihai Fe deposit in Hami, Xinjiang. Internal data (in Chinese).
Li, C., Zhang, M., Fu, P., Qian, Z., Hu, P., Ripley, E.M., 2012. The Kalatongke magmatic Ni-Cu deposits in the Central Asian Orogenic Belt, NW China: product of slab window magmatism? Miner. Deposita 47, 51–67.
Lin, J.L., Xia, M.Z., Guo, X.N., Wang, B.Y., Xia, Z.D., Jiang, C.Y., 2011. Petrogenesis of Luodong mafic-ultramafic layered intrusion, Beishan region, Xinjiang. Geochim. Cosmochim. Acta 40 (6), 499–515 (In Chinese with English abstract).
Liu, Y.S., Hu, Z.C., Gao, S., Günther, D., Xu, J., Gao, C.G., Chen, H.H., 2008. In situ analysis of major and trace elements of anhydrous minerals by LA-ICP-MS without applying an internal standard. Chem. Geol. 257, 34–43.
Liu, Y.S., Gao, S., Hu, Z., Gao, C., Zong, K., Wang, D., 2010. Continental and oceanic crust recycling-induced melt-peridotite interactions in the Trans-North China Orogen: U-Pb dating, Hf isotopes and trace elements in zircons of mantle xenoliths. J. Petrol. 51, 537–571.
Liu, Y.R., Lv, X.B., Mei, W., Dai, Y.C., 2012. Mineralogy of clinopyroxene from Pobei mafic-ultramafic complex in Beishan area, Xinjiang, and its geological significance. Acta Petrol. Miner. 31 (2), 212–214 (In Chinese with English abstract).

Liu, P.P., Zhou, M.F., Wang, C.Y., Xing, C.M., Gao, J.F., 2014. Open magma chamber processes in the formation of the Permian Baima mafic-ultramafic layered intrusion, SW China. Lithos 184, 194–208.
Mallmann, G., O'Neil, H.S.C., 2009. The crystal/melt partitioning of V during mantle melting as a function of oxygen fugacity compared with some other elements (Al, P, Ca, Sc, Ti, Cr, Fe, Ga, Y, Zr and Nb). J. Petrol. 50 (9), 1765–1794.
Mao, Y.J., 2014. Petrogenesis and ore genesis of the multiphase mafic-ultramafic intrusions in the Huangshan Ni-Cu ore camp, Eastern Tianshan, south Central Asian Orogenic Belt (CAOB) (Ph.D dissertation). Cartography and Geography Information System, Economic deposit, p. 149 (In Chinese with English abstract).
Mazzucchelli, M., Rivalenti, G., Vannucci, R., Bottazzi, P., Ottolini, L., Hofmann, A.W., Parenti, M., 1992. Primary positive Eu anomaly in clinopyroxenes of low-crust gabbroic rocks. Geochim. Cosmochim. Acta 56, 2363–2370.
Melluso, L., Lustrino, M., Ruberti, E., Brotzu, P., Amelio, F., 2008. Major- and trace-element composition of olivine, perovskite, clinopyroxene, Cr-Fe-Ti oxides, phlogopite and host kamafugites and kimberlites, Alto Paranaiba, Brazil. Can. Mineral. 46, 19–40.
Meng, Q.P., Chai, F.M., Li, Q., Zheng, J.H., Shao, F.Z., Geng, X.X., Han, W.Q., 2014. Zircon U-Pb geochronology, Hf isotopes and the petrogenesis of mafic intrusions in the Cihai Fe (-Co) deposit, Xinjiang. Acta Petrol. Sin. 30 (1), 109–124 (In Chinese with English abstract).
Morimoto, N., 1988. Nomenclature of pyroxenes. Mineral. Petro. 39, 55–76.
Naldrett, A.J., 1999. World class Ni-Cu-PGE Deposits: Key factors in their genesis. Mineral. Deposita 34, 227–240.
NGPBMMI (Northwest Geological Prospecting Bureau of the Ministry Metallurgical Industry), 1999. The geological exploration report of open-pit Cihai Fe deposit II, Hami, Xinjiang. Interal data (in Chinese).
Nimis, P., 1995. A clinopyroxene geobarometer for basaltic systems based on crystal-structure modeling. Contrib. Mineral. Petrol. 121, 115–125.
Nimis, P., Ulmer, P., 1998. Clinopyroxene geobarometry of magmatic rocks Part 1: An expanded structural geobarometer for anhydrous and hydrous, basic and ultrabasic systems. Contrib. Mineral. Petrol. 133, 122–135.
Nisbet, E.G., Pearce, J.A., 1977. Clinopyroxene composition in mafic lavas from different tectonic settings. Contrib. Mineral. Petrol. 63, 149–160.
Obsorne, E.F., 1959. Role of oxygen pressure in the crystallisation and differentiation of basaltic magmas. Am. J. Sci. 257, 609–647.
Pan, J.H., Guo, Z.J., Liu, C., Zhao, Z.H., 2008. Geochronology, geochemistry and tectonic implications of Permian basalts in Hongliuhe area on the border between Xinjiang and Gansu. Acta Petrol. Sin. 24, 793–802 (In Chinese with English abstract).
Pang, K.N., Zhou, M.F., Lindsley, D., Zhao, D.G., Malpas, J., 2008. Origin of Fe-Ti oxide ores in mafic intrusions: Evidence from the Panzhihua intrusion, SW China. J. Petrol. 49 (2), 295–313.
Peach, C.L., Mathez, E.A., 1993. Sulfide melt-silicate melt distribution coefficients for nickel and iron and implications for the distribution of other chalcophile elements. Geochim. Cosmochim. Acta 57, 3013–3021.
Qi, T.J., Xue, C.J., Zhang, Z.C., Wang, Y.H., Shao, F.Z., 2012. Basic igneous rock in Cihai giant iron district, Hami, Xinjiang, and its indication to the Metallogenic setting. Earth Sci. J. China Uni. Geosci. 37 (6), 1315–1326 (In Chinese with English abstract).
Qian, Q., O'Neill, H.S.C., Hermann, J., 2010. Comparative diffusion coefficients of major and trace elements in olivine at ~950°C from a xenocryst included in dioritic magma. Geology 38, 331–334.
Qin, K.Z., Zhang, L.C., Xiao, W.J., 2003. Overview of major Au, Cu, Ni and Fe deposits and metallogenic evolution of the eastern Tianshan Mountains, Northwestern China. In: Mao, J.W., Goldfarb, R.J., Seltrnan, R. (eds.).Tectonic evolution and metallogeny of the Chinese Altay and Tianshan (London), 227-249.
Reynolds, I.M., 1980. Ore petrography and mineralogy of the vanadium-bearing titaniferous magnetite layer of the Kaffirskraal intrusion, Heidelberg district. Transvaal. Transac. Geol. Soc. South Africa 83, 221–230.
Ripley, E.M., 1981. Sulfur isotopic abundances of the Dunka Road Cu–Ni deposit, Duluth Complex, Minnesota. Econ. Geol. 76, 619–620.
Rojas-Agramonte, Y., Kröner, A., Demoux, A., Xia, X., Wang, W., Donskaya, T., Liu, D., Sun, M., 2011. Detrital and xenocrystic zircon ages from Neoproterozoic to Paleozoic arc terranes of Mongolia: Significance for the origin of crustal fragments in the Central Asian Orogenic Belt. Gondwana Res. 19, 751–763.
Rudnick, R.L., 1992. Restites, Eu anomalies, and the lower continental crust. Geochim. Cosmochim. Acta 56, 963–970.
Rudnick, R.L., Gao, S., 2003. Composition of the continental crust. In: Rudnick, R.L. (Ed.), Treatise on Geochemistry Volume 3: The Crust. Elsevier, pp. 1–64.
Shellnutt, J.G., Zhou, M.F., Zellmer, G.F., 2009. The role of Fe-Ti oxide crystallization in the formation of A-type granitoids with implications for the Daly gap: An example from the Permian Baima igneous complex, SW China. Chem. Geol. 259, 204–217.
Su, B.X., Qin, K.Z., Sakyi, P.A., Li, X.H., Yang, Y.H., Sun, H., Tang, D.M., Liu, P.P., Xiao, Q. H., Malaviarachchi, S.P.K., 2011. U-Pb ages and Hf-O isotopes of zircons from Late Paleozoic mafic-ultramafic units in the southern Central Asian Orogenic Belt: Tectonic implications and evidence for an Early-Permian mantle plume. Gondwana Res. 20, 516–531.
Su, B.X., Qin, K.Z., Sun, H., Tang, D.M., Sakyi, P.A., Chu, Z.Y., Liu, P.P., Xiao, Q.H., 2012. Subduction-induced mantle heterogeneity beneath Eastern Tianshan and Beishan: Insights from Nd-Sr-Hf-O isotopic mapping of Late Paleozoic mafic-ultramafic complexes. Lithos 134–135, 41–51.
Sun, H., 2009. Ore-forming Mechanism in Conduit System and Ore-bearing Property Evaluation for mafic-ultramafic Complex in Eastern Tianshan, Xinjiang (Ph.D dissertation). Institute of Geology and Geophysics, Chinese Academy of Sciences, p. 262 (In Chinese with English abstract).
Sun, S.S., McDonough, W.F., 1989. Chemical and isotopic systematics in ocean basalt: implication for mantle composition and processes. In: Saunders, A.D., Norry, M.J. (Eds.), Magmatism in the Ocean Basins. Geological Society of London Special Publications 42, pp. 313–345.
Sverjensky, D.A., 1984. Europium redox equilibria in aqueous solution. Earth Planet. Sci. Lett. 67, 70–78.
Tang, P.Z., Wang, J.B., Wang, Y.W., Long, L.L., 2010. Geochemical characteristics of mafic-ultramafic rocks in the Cihai ore district, Xinjiang, and their geological significance. Geochim. Cosmochim. Acta 39 (6), 542–552 (In Chinese with English abstract).
Tang, P.Z., Wang, Y.W., Wang, J.B., Long, L.L., Liao, Z., 2012. Geochemical characteristics of cobalt from the Cihai ore district, Xinjiang, and their significance. Acta Miner. Sin. 32 (3), 379–385 (In Chinese with English abstract).
Taylor, R.W., 1963. Liquidus temperatures in the system $FeO-Fe_2O_3-TiO_2$. J. Am. Ceramic Soci. 46, 276–279.
Tegner, C., Cawthorn, R.G., Kruger, F.J., 2006. Cyclicity in the main and upper zones of the Bushveld Complex, South Africa: crystallization from a zoned magma sheet. J. Petrol. 47, 2257–2279.
Tian, W., Campbell, I.H., Allen, C.M., Guan, P., Pan, W., Chen, M., Yu, H., Zhu, W., 2010. The Tarim picrite-basalt-rhyolite suite, a Permian flood basalt from northwest China with contrasting rhyolites produced by fractional crystallization and anatexis. Contrib. Mineral. Petrol. 160, 407–425.
Toplis, M.J., Corgne, A., 2002. An experimental study of element partitioning between magnetite, clinopyroxene and iron-bearing silicate liquids with particular emphasis on vanadium. Contrib. Mineral. Petrol. 144, 22–37.
Wang, C.Y., Zhou, M.F., Zhao, D.G., 2008. Fe-Ti-Cr oxides from the Permian Xinjie mafic-ultramafic layered intrusion in the Emeishan large igneous province, SW China: crystallization from Fe- and Ti-rich basaltic magmas. Lithos 102, 198–217.
Weill, D.F., Drake, M.J., 1973. Europium anomaly in plagioclase feldspar: Experimental results and semiquantitative model. Science 180, 1059–1060.
Wilmart, E., Demaiffe, D., Duchesne, J.C., 1989. Geochemical constraints on the genesis of the Tellnes ilmenite deposit (SW Norway). Econ. Geol. 84, 1047–1056.
Windley, B.F., Alexeiev, D., Xiao, W.J., Kröner, A., Badarch, G., 2007. Tectonic models for accretion of the Central Asian Orogenic Belt. J. Geol. Soc. Lond. 164, 31–47.
Witt-Eckschen, G., O'Neill, H.S.C., 2005. The effect of temperature on the equilibrium distribution of trace elements between clinopyroxene, orthopyroxene, olivine and spinel in upper mantle peridotite. Chem. Geol. 221, 65–101.
Wong, K., Sun, M., Zhao, G.C., Yuan, C., Xiao, W.J., 2010. Geochemical and geochronological studies of the Alegedayi Ophiolitic Complex and its implication for the evolution of the Chinese Altai. Gondwana Res. 18, 438–454.
Xia, L.Q., Xu, X.Y., Li, X.M., Ma, Z.P., Xia, Z.C., 2012. Reassessment of petrogenesis of Carboniferous-Early Permian rift-related volcanic rocks in the Chinese Tianshan and its neighboring areas. Geosci. Front. 3, 445–471.
Xia, M.Z., Jiang, C.Y., Li, C.S., Xia, Z.D., 2013. Characteristics of a newly discovered Ni-Cu sulfide deposit hosted in the Poyi ultramafic intrusion, Tarim Craton, NW China. Econ. Geol. 108, 1865–1878.
Xiao, Q.H., 2010. Origin of Xianghshanxi Cu-Ni-Ti-Fe Composite Deposit in Eastern Tianshan, NW China, and Its Implications (Ph.D dissertation). Institute of Geology and Geophysics, Chinese Academy of Sciences, p. 191 (In Chinese with English abstract).
Xiao, W.J., Windley, B.F., Hao, J., Zhai, M.G., 2003. Accretion leading to collision and the Permian Solonker suture, Inner Mongolia, China: Termination of the central Asian orogenic belt. Tectonics. http://dx.doi.org/10.1029/2002TC001484.
Xiao, W.J., Zhang, L.C., Qin, K.Z., Sun, S., Li, J.L., 2004. Paleozoic accretionary and collisional tectonics of the eastern Tianshan (China): Implications for the continental growth of central Asia. Am. J. Sci. 304, 370–395.
Xiao, W.J., Windley, F., Huang, B.C., Han, C.M., Yuan, C., Chen, H.L., Sun, M., Sun, S., Li, J.L., 2009. End-Permian to mid-Triassic termination of the accretionary processes of the southern Altaids: implications for the geodynamic evolution, Phanerozoic continental growth, and metallogeny of Central Asia. Int. J. Earth Sci. 98, 1189–1217.
Xiao, W.J., Windley, B.F., Allen, M.B., Han, C.M., 2013. Paleozoic multiple accretionary and collisional tectonics of the Chinese Tianshan orogenic collage. Gondwana Res. 23 (4), 1316–1341.
Xu, X.Y., He, S.P., Wang, H.L., Chen, J.L., 2009. Geological Background Map of Mineralization in Eastern Tianshan-Beishan Area (in Chinese).
Xue, C.J., Ji, J.S., Yang, Q.J., 2000. Subvolcanic hydrothermal metallogeny of the Cihai iron (cobalt)deposit Xinjiang. Miner. Deposita 19 (2), 156–164 (In Chinese with English abstract).
Xue, S.C., Qin, K.Z., Li, C.S., Tang, D.M., Mao, Y.J., Qi, L., Ripley, E.M., 2016. Geochronological, petrological, and geochemical constraints on Ni-Cu sulfide mineralization in the Poyi ultramafic-troctolitic intrusion in the northeast rim of the Tarim Craton, western China. Econ. Geol. 111, 1465–1484.
Yang, S.F., Li, Z.L., Chen, H.L., Chen, W., Yu, X., 2006. ^{40}Ar-^{39}Ar dating of basalts from Tarim Basin, NW China and its implication to a Permian thermal tectonic event. J. Zhejiang Univ. Sci. 7, 30–324 (In Chinese with English abstract).
Yang, S.F., Yu, X., Chen, H.L., Li, Z.L., Wang, Q.H., Luo, J.C., 2007. Geochemical characteristics and petrogenesis of Permian Xiaohaizi ultrabasic dyke in Bachu area, Tarim basin. Acta Petrol. Sin. 23 (5), 1087–1096 (In Chinese with English abstract).

Yang, W.C., Wang, J.L., Zhong, H.Z., Chen, B., 2012. Analysis of regional magnetic field and source structure in Tarim Basin. Chi. J. Geophys. 55, 1278–1287 (In Chinese with English abstract).
Yogodzinski, G.M., Kelemen, P.B., 2007. Trace elements in clinopyroxenes from Aleutian xenoliths: Implications for primitive subduction magmatism in an island arc. Earth Planet. Sci. Lett. 256, 617–632.
Zhang, L.F., Ellis, D.J., Jiang, W., 2002. Ultrahigh pressure metamorphism in western Tianshan, China, part I: Evidences from the inclusion of coesite pseudomorphs in garnet and quartz exsolution lamellae in omphacite in eclogites. Am. Miner. 87, 853–860.
Zhang, Z.C., Zhou, G., Kusky, T.M., Yan, S.H., Chen, B., Zhao, L., 2009. Late Paleozoic volcanic record of the Northern Junggar Terrane, Xinjiang: Major and trace elment characteristics, Sr-Nd isotopic systems and implications for tectonic evolution. Gondwana Res. 16, 201–215.
Zhang, C.L., Xu, Y.G., Li, Z.X., Wang, H.Y., Ye, H.M., 2010a. Diverse Permian magmatism in the Tarim Block, NW China: genetically linked to the Permian Tarim mantle plume? Lithos 119, 537–552.
Zhang, Y.T., Liu, J.Q., Guo, Z.F., 2010b. Permian basaltic rocks in the Tarim basin, NW China: Implications for plume-lithosphere interaction. Gondwana Res. 18, 596–610.
Zhang, C.L., Zou, H.B., Li, H.K., Wang, H.Y., 2012. Tectonic framework and evolution of the Tarim block in NW China. Gondwana Res. http://dx.doi.org/10.1016/jgr.2012.05.009.
Zhong, H., Zhou, X.H., Zhou, M.F., Sun, M., Liu, B.G., 2002. Platinum-group element geochemistry of the Hongge Fe-V-Ti deposit in the Pan-Xi area, southwestern China. Miner. Deposita 37, 226–239.
Zhou, M.F., Robinson, P.T., Lesher, C.M., Keays, R.R., Zhang, C.J., Malpas, J., 2005. Geochemistry, petrogenesis and metallogenesis of the Panzhihua gabbroic layered intrusion and associated Fe-Ti-V oxide deposits, Sichuan province, SW China. J. Petrol. 46 (11), 2253–2280.
Zhou, D.W., Liu, Y.Q., Xin, X.J., Hao, J.R., Dong, Y.P., Ouyang, Z.J., 2006. Formation of the Permian basalts and implications of geochemical tracing for paleo-tectonic setting and regional tectonic background in the Turpan-Hami and Santanghu basins, Xinjiang. Sci. China (D) 49, 584–596 (In Chinese with English abstract).
Zirner, A.L.K., Marks, M.A.W., Wenzel, T., Jacob, D.E., Markl, G., 2015. Rare earth elements in apatite as a monitor of magmatic and metasomatic processes: The ilimaussaq complex, South Greenland. Lithos 228–229, 12–22.